Bearing capacity of a shallow foundation on several types of ground with cavity under dry and unsaturated conditions based on Rigid Plastic Finite Element Method

By

KEBA LUKUETA Eric

A thesis submitted in partial fulfillment of the requirements for the degree of Doctor of Philosophy in Engineering

Supervision and Guidance: **Prof. Koichi Isobe**

Examination committee:

Prof. Koichi ISOBE

Prof. YOICHI WATABE

Prof. SATOSHI NISHIMURA

Thesis No.

Division of Field Engineering for Environment

Graduate School of Engineering, Hokkaido University

June 2024

Dedication

To the ones who lit the path and walked beside me through the labyrinth of academia: my family, whose unwavering support and understanding made every step possible; my mentors and advisors, whose guidance and wisdom shaped my scholarly journey; and to my friends and colleagues, who shared both the challenges and triumphs along the way. This work is dedicated to each of you, for your belief in me never stumbled, and your encouragement never faded.

Acknowledgement

I would like to express my deepest gratitude to the Ministry of Education, Culture, Sports, Science and Technology (MEXT) of Japan for their invaluable support with a scholarship throughout my doctoral journey. My heartfelt appreciation goes to my dedicated supervisor Koichi Isobe, whose guidance, encouragement, and expertise have been instrumental in shaping this thesis. I am profoundly thankful to my loving family—my wife Micheline and two daughters (Joyce and Zoe)—for their unwavering support, understanding, and patience during the challenging phases of this academic pursuit. A special thank you to my parents for their unwavering investment in my education and their continuous prayers. I wish to express my deep appreciation to my siblings; their encouragements helped me pass through these years away from home. This achievement would not have been possible without the collective support of these remarkable individuals and institutions. Thanks for your patience and sacrifice to make this work come to an end.

Abstract

Ensuring the stability and load-bearing capacity of shallow foundations is critical for the safety and durability of various structures. However, when these foundations are situated on ground containing voids like underground karst features or voids from natural or human-induced processes, their behavior becomes considerably more intricate. Understanding the interaction between shallow foundations and such cavity-prone ground is essential for engineers and geotechnical practitioners in designing resilient and dependable structures. This study aims to investigate the bearing capacity of shallow foundations on ground with cavities, considering various soil properties to delineate zones of influence on the foundation and consequently design robust foundations for challenging soil conditions. Through this research, we have conducted a thorough analysis of the Ultimate Bearing Capacity utilizing

a numerical analysis code developed within our research group, known as the Rigid Plastic Finite Element Method (RPFEM). This endeavor seeks to offer valuable insights to enhance the design and performance of shallow foundations while elucidating the influence zones in regions susceptible to subsurface cavities. In this study, the investigation is structured into three distinct steps, each aimed at illuminating different aspects of the problem. (1) Initially, an analysis of the Ultimate Bearing Capacity (UBC) under dry conditions is conducted, focusing on undrained scenarios to comprehend how the foundation behaves when there is no water flow within the soil. (2) Subsequently, we delved into the analysis of the UBC under unsaturated conditions, acknowledging the influence of moisture content on soil strength and its implications for foundation performance. (3) Finally, experimental methods were employed to complement theoretical analyses, offering empirical validation and deeper insights into the complex interactions between shallow foundations and ground containing cavities. Through this systematic approach, the goal is to provide a comprehensive understanding of the bearing capacity of shallow foundations in challenging soil environments characterized by the presence of subsurface cavities.

(1) In the analysis conducted under dry conditions, which encompasses various soil types such as cohesive and intermediate soils, the results are presented using dimensionless 2D

charts. These charts feature normalized horizontal axis X and vertical axis Y, which are horizontal and vertical distances of the cavity to the footing normalized to the parameters R and H respectively. R and H represent the horizontal and vertical extents of the boundaries of the failure surface beneath the footing in the absence of the soil cavity. By examining geometric factors like footing width B and cavity characteristics (shape, size, and location), the study illustrates that the farther the cavity is, the lesser its impact on the footing's performance. The distribution of normalized bearing capacity across the (X, Y) space elucidates the expansion and variation of the influence zone. Equations incorporating the aforementioned geometric parameters and soil shear strengths are proposed and validated using literature data, with adjustments made according to the different soil types involved.

(2) The analysis conducted under unsaturated conditions examined the geometric parameters of the footing and the cavities, similar to the approach taken in the dry conditions analysis. The primary focus was on evaluating the effects of matric suction and instability of the cavity itself on the overall performance of the footing under these specific conditions. Given the recent advancements in unsaturated soil mechanics and the prevalence of foundations existing in unsaturated conditions throughout their lifespan, predicting the behavior of the footing-cavity system under such hydraulic conditions is considered crucial. The Soil-Water Characteristic Curve (SWCC) model utilized was the van Genuchten model due to its simplicity and effectiveness. The results of the seepage analysis unveiled various distributions of porewater pressure heads depending on the cavity location. Despite similarities in the conclusions drawn from the Ultimate Bearing Capacity (UBC) analysis compared to the dry conditions, there was a notable expansion observed in the zone of influence. Furthermore, failure mode analyses highlighted the differences and influence of matric suction in unsaturated conditions. Equations describing the influence zone incorporating geometric parameters and soil shear strength parameters are also provided.

(3) The experimental approach encompassed a laboratory-scale simulation method to replicate the presence of a cavity and its effects on the ultimate bearing capacity of the footing. The experiments included generating cavities from their initial state and studying their

respective impacts. Model footing tests were performed on unsaturated sandy soil containing a simulated cavity. The cavity was created using a readily available commercial balloon, which was inserted into the model soil and then expanded. Following the deflation of the balloon, the unsaturated soil was vertically loaded using a circular model footing with a diameter of B = 30 mm. Through the experimental results, the validity of the numerical analyses, particularly under unsaturated conditions, was successfully confirmed.

In light of our comprehensive study, which findings elucidated the impact and range of the ultimate bearing capacity of a shallow foundation situated on ground containing cavities under different soil and hydraulic conditions. It is imperative that construction practitioners and regulatory bodies recognize the potential impact of subsurface voids on the stability of foundations. Our findings underscore the need for applying straightforward formulas based on the soil types, geometry, and hydraulic conditions to assess the stability level when a cavity is discovered. Such solutions are scarce in the current literature and such solution is proposed in the current work. Moreover, these results are anticipated to offer practical insights, including identifying areas that require investigation for the presence of cavities.

Table Of Contents

List of figures

List of tables

Abbreviations

- RPFEM = Rigid Plastic Finite Element Method
- FEM = Finite Element Method
- UBC = Ultimate Bearing Capacity
- BC = Bearing Capacity
- SWCC: Soil water characteristic curve
- WT: Water table

Symbols

- B: Footing width.
- c: Soil cohesion.
- ϕ: Shear resistance angle.
- γ: Unit weight of the soil.
- h: Vertical gap between the ground surface and the cavity's center.
- D: Diameter of the cavity.
- r: Horizontal distance between the centerlines of the cavity and the footing.
- BC/BC_{NV}: Ratio of the footing's bearing capacity on soil with a cavity to the bearing capacity of footing on soil without a cavity.
- R: Normalization parameter representing the horizontal size of the plastic region (failure surface) beneath the footing on soil without cavity.
- H: Normalization parameter representing the vertical size of the plastic region (failure surface) beneath the footing on soil without cavity.
- $X = (r\text{-}D/2/R)$: Horizontal axis of the influence zone representing the horizontal distance of the cavity to the footing normalized with the parameter R.
- $Y = (h\text{-}D/2/H)$: Vertical axis of the influence zone representing the vertical distance of the cavity to the soil surface normalized with the parameter H.
- p and q: Coefficients of the equation of the zone of influence, function of the shear resistance angle and cohesion.
- $a_0, a_1, a_2, b_0, b_1, b_2$: Coefficients of the equation of the zone of influence (expressed as a function of the cohesion ($c/\gamma B$).
- θ_r: Residual volumetric moisture content.
- θ_s: Saturated volumetric water content.
- k: Permeability coefficient.
- n: Van Genuchten parameter
- D_t: Inner diameter of the circular base of the experimental acrylic apparatus.

- D_r: relative density of the soil sample

Chapter 1. Introduction

1.1 Background

Underground cavities occur as the results of natural causes, manmade causes or sometimes a complex combination of both. The natural occurrence of the cavities is due to mainly the geological settings of underlying rocks, especially soluble rocks such as limestone, dolomite chalk, gypsum. In this type of the geomaterials, the creation of the cavity, is a complex combination of chemical erosion, that goes on through a certain period of times (usually geological times), and mechanical erosion. The chemical erosion usually generates a network of underground cavities with icicles shape-like deposits such as Stalactites and stalagmites. The manmade cavities type origins differ according the type of human activities: Mining, abandoned quarries, Tunnelling, Defective pipes, pumping, etc. Their growth, is subject to the progression of the internal erosion which evolves or expands from an initial cavity. The infiltration waters and rate are of paramount influence in the acceleration of the process that induces surface subsidence or collapse known as sinkholes.

The cavities expanding within the soil, after overreaching the bearing capacity of the bearing layers can lead to subsidence, collapse of the overburden. This occasionate often casualty in urban areas of several types: Building collapse, Engineering structures, farm land, flooding, etc. in brief, every human crafted work. The serious damages can induce economic loss, loss human lives, etc. (Hermosilla, 2012). Sinkholes/ subsidence displays a wide range morphology: cylindrical, conical, bowl-or-pan shaped. They vary in size ranging from a few cm up to hundreds of meters across. Figure 1-1 illustrates the expansion of the cavity within the ground and Figure 1-2 illustrates images of the cavities collapse around the world.

With the population growth worldwide, more and more people are prone on building or settling on the unstable ground. Solutions to preventing collapse of discovered underground cavities such as grouting, filling with other materials exist. However, not all residents afford these implementations. In some case, the collapse is retarded due to the shear strength of the soil. The site investigation ahead of the land development can reveal underground cavity

which influence on the structures is sometimes not well defined to indefinite shape and size and eventually other uncertainties. In addition, the treatment methods are not usually planned on site. Thus, it is necessary to determine a way of determining the influence of the cavity on the engineering structures.

(a) Large sinkhole in Fukuoka, Japan (2016). Source BBC news

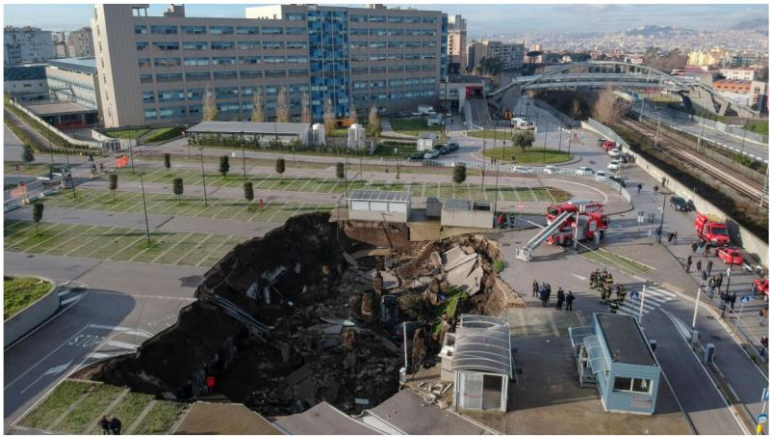

(b) Massive sinkhole near an Italian hospital in Napoli, Italy (2021). Source: CNN.

(c) Open sinkhole in Florida, USA (https://water.usgs.gov/edu/sinkholes.html). Source BBC news

(d) Collapse due to rainwater leaking through pavement and carrying soil into a ruptured sewer pipe. Source: https://handwiki.org/wiki/Earth:Sinkhole

(e) Sinkhole in the city of Mbuji-Mayi, (DR of Congo)

Figure 1-2. Sinkholes occurrence

Several Authors have tackled the issues of underground based on different approach. The studies of sinkholes with an emphasis on the monitoring of the ground surface settlement have been undertaken by Aliet al., 2020 using small version of small scale of the physical models in experiments. Much of the literature on the subject have been empirical in nature, often associated with a specific location.

1.2 Research Objectives

The bearing capacity of shallow foundation is a non-negligible issue in the geotechnical engineering community. The routine design of the shallow foundation is usually based on the conventional saturated soil mechanics. However, the progress in recent years in the unsaturated soil mechanics have been emphasizing the effects of increased shear strength of soils in unsaturated states thanks to the generation of the soil suction (Garakani et al., 2020; Costa et al., 2003; Rojas et al., 2007; Tang et al., 2018; Vanapalli & Mohamed, 2013).Therefore, it is more than important to assess the performance of the shallow foundation in the presence of underground cavity in order to have realistic solutions or design.

The study investigates the influence of underground cavity within several types of soil by analyzing the ultimate bearing capacity of a shallow foundation resting on the soil with cavity. The assumption of dry and unsaturated conditions is made to analyze the UBC of the

footing in order to identify the influence of several shear strengths parameters and, consequently the influence zone extension/variation based on shear strength parameters based on the assumptions of the conventional soil mechanics as well as the unsaturated soil mechanics. Analyses of the compared failure modes are carried out and interesting observation are made upon thorough investigations.

1.3 Research method

The present study is carried out through the use the Rigid Plastic Finite Element Method RPFEM which has been used in several published original papers and research works for the Analyses of the UBC of the shallow foundation as well pile foundations. The RPFEM which detailed equations and advantages will be introduced later.

Secondly, to achieve the objectives of this study, several models' tests have been conducted. These are conducted on the sandy dry and unsaturated soils. The cavity within the soil has been simulated with an inflated balloon and simulate an existing and grown cavity. In addition, the effects of a cavity at initial occurrence are investigated through the flowing of sand and water through a tiny orifice that illustrate an internal erosion.

1.4 Thesis Outline

Except the Conclusions and suggestions, this thesis is composed of five chapters including the introduction.

The chapter 2 is a comprehensive review of the literature of the studies related to the stability of structures in presence of underground cavities. The studies focused on describing the mechanisms of underground cavities, and sinkholes are reviewed. In addition, some other studies related to the analysis of stability of engineering structures, and finally those involved in the prediction of risk and collapse analysis are analyzed to provide a general foundation for the understanding of the influence of the cavity within the soil.

The chapter 3 and 4 introduce the analyses of the ultimate bearing capacity of shallow foundation on soil with cavity. Throughout these chapters details of the constitutive equations

of the RPFEM are provided. These chapters are the main core of this thesis as they are parts of our published research paper and work to be publish.

The chapter 5 is devoted to experimental study and analysis of the UBC of a footing on soil with a cavity. An introduction of the developed method of analysis is introduced. The several cases of analyses considering the cavity vertical location, the initial stage or grown stage of a cavity is simulated while creating unsaturated conditions.

The chapter 6 provides some general conclusions and recommendations for the future research work.

Chapter 2. Literature Review

2.1 Introduction

Studies on underground cavities cover a wide range of disciplines and research focuses. These studies can demonstrate the interdisciplinary nature portraying diverse interests and applications across scientific, environmental, engineering and cultural domain. They can be grouped based on their research focus, methods and applications as below.

The ***Geological studies***, which employs geophysical surveys, geological mapping, seismic studies, borehole investigations to understand the geological formation and characteristics of underground cavities. Their applications are found in the identification of the types of rock formations, assessing the stability of cavities, predicting potential hazards (Ford and Williams, 2007). The ***Hydrogeological studies*** focus on investigating the water flow and hydrological aspects of underground cavities. These studies model groundwater, run tracer tests and water quality analysis with the aim of understanding the groundwater recharge, aquifer behavior, etc. (Freez, R.A. and Jacob, C.V., 1979). ***The engineering and Infrastructures studies*** use methods of geotechnical assessments, subsurface imaging and structural analysis to evaluate the impact of underground cavities on infrastructures and engineering projects. The applications of such studies are about the ensuring of the stability of buildings, tunnels, and other structures. They also contribute in the mitigation of risk associated with subsurface voids (Duncan, 2000; Goodman, 1989; Terzaghi et al., 1996).

The ecological studies group are involved in the ecological aspects associated with the underground cavities on surrounding environments. They assess biodiversity, habitats and conduct ecological modeling. These studies 'emphasis is on the understanding of the role cavities in the ecosystems, conservation efforts, etc. (Culver et al., 2019).

The other group is the one ***Archeological study*** which employ ground-penetrating radar, remote sensing and excavation methods. The exploration of underground cavities for archeological purposes is the main focus. These studies lead to discovering historical sites, artifacts, and cultural heritage hidden in subterranean spaces (Renfrew and Bahn, 2018).

The studies of cave exploration and Speleology study caves and underground passages for recreational, scientific, and conservation purposes. The cave mapping, speleothem analysis and exploration expeditions are the methods used (Palmer, 2007). The studies related to the ***Resource Exploration*** which investigate the underground cavities for potential resources such as minerals, oils, or gas. With the aim of identifying economic opportunities, resource extraction, and sustainable resource management, these studies also employ geophysical surveys, drilling and mineralogical analysis (Machel et al., 1986). The studies related to ***risk assessment and Management***. Within the range of these studies, the assessment and mitigation of risk associated with underground cavities are accentuated. These studies are applied to minimize the impact of subsurface hazards on human safety, infrastructure and the environment (Chandler et al., 2008; Hoek et al., 2002; Varnes, 1984)(Lee. H. and Jones, J. 2004). As describe above, the cavity related problem has been tackled over a range of disciplines, each with its specific methods and goals. The current work is in the range of ***Engineering and Infrastructures studies***. The following lines are dedicated to a comprehensive literature review of works analyzing through numerical analysis and experimental analysis the bearing capacity of a shallow foundations above the soil with cavity.

2.2 Studies of Stability analysis and Bearing capacity of strip footings above soil with cavity

The traditional approach to predicting cavity collapse in soil, as opposed to the problem of locating the cavities themselves, has been to use physical modeling and analytical techniques. The precursor studies on the topic were conducted by (Baus and Wang, 1984). They conducted an experimental and analytical investigation of the bearing capacity of the footing above cavity on silty clay using a finite element method considering the soil as an elastic perfectly plastic material. They found that for each footing there exists a critical depth below which the presence of a cavity has a negligible impact on the performance of the footing Badie et al., (1984). When the void is located above the critical depth, the bearing capacity varies with various factors such as the size and location of the void and the depth of the

foundation. However, the influence zone expansion is depending on several parameters as mentioned but no clear combinations of these variations are illustrated in their study.

Wang and Hsieh, (1987) used an upper bound limit analysis and calculated the bearing capacity of strip footing centered above the circular voids. They proposed a complex equation which required nonlinear approach to be solved. Another analytical approach to sinkhole formation was developed by Tharp, (1999) who studied the likely expansion of a cavity leading to a sinkhole, including the effects of pore–water pressure changes. His analysis consisted of steps starting with a linear elastic, isotropic stress field in the soil around a cavity, followed by steps in which the development of radial cracks and loss of soil into the cavity. Tharp, (1999) concluded that steady-state groundwater conditions should generally promote stability and that sinkhole formation resulting from rapid drawdown of the water table could be avoided by sufficiently slow lowering.

Other researchers interested in the stability of lined and unlined tunnels (Atkinson and Potts, 1977; Davis et al., 1980; Leca and Dormieux, 1990; Mühlhaus, 1985) worked in the similar aspects to evaluate stability of submerged cavity. Davis et al., (1980) studied the stability of lined tunnels in rigid plastic soil where the unsupported face was pressurized. A centrifuge testing and analytical approaches based on the Method of Characteristics and limit analysis were used. Their results showed that the bound theorems of classical plasticity was the techniques yielding the widest range of solutions for this problem. Davis et al., (1980) deduced rigorous bounds for undrained collapse loads for plane strain headings, plane strain tunnels, and circular headings, which are similar problems to that of a submerged cavity collapse. Drumm et al., (2009) used limit analysis to investigate the stability of a vertical cylindrical shaft in soil above bedrock, modeling a sinkhole immediately as it had formed and before subsequent collapse to form a funnel-shaped depression. However, this is a of the situation once a submerged cavity has collapsed and is thus, is of little relevance to this work.

Augarde et al., (2003) used the numerical modeling, namely the Limit Analysis method, to study the undrained stability of the submerged cavities that leads to sinkhole formation. The FEM limit Analysis provided upper and lower bound values of a suitable load parameter,

bracketing the exact solution. They proposed equations taking in account the dimensionless parameters of depth of cavity, diameter of the cavity, unit weight, and the undrained shear resistance of the clay. In addition, they found that failure was dominated by local collapse, due to the need to enforce associated flow in the limit analysis procedures. The work by Augarde et al., (2003) were retaken by Keawsawasvong et al., (2019) considering cohesive soils. They conducted a parametric study of undrained stability of a spherical cavity in clays using finite element limit analysis with axisymmetric condition. The influences of cover depth ratio of cavity and dimensionless overburden factor on predicted failure mechanisms and dimensionless load factor were examined. Their update the studied the previous studies and improved the accuracy of the solutions based on the nonlinear regression analysis of a computed average bound solutions. The solution is mainly an expression of what is called Stability factors as function of soil cohesion and unit weight. However, these solutions are punctual and limited to cavities centered with the load application points. Or, in nature, the cavity causing performance decreasing can be also eccentric with the loading application point. Therefore, it is necessary to analyze the stability in the case of eccentric cavity.

2.3 Experimental analysis and simulation of the soil with cavity

Craig (1990), Abdulla and Goodings (1996) investigated the stability of soils over cavities through centrifuge modeling. Within these experiments, they used configurations idealized as cavities and collapse was obtained from the overburden weight alone. Craig (1990), used a cylindrical cavity opened up in a two layered clay soil and tested in two steps. The first step consisted in increasing the overburden weight gradually as well as the speed of the centrifuge failure of clay. The second step or type of test, the centrifuge speed was kept constant and the sand was removed from the void beneath the clay layers. Craig found adequation in the assumption of a simple cylindrical rigid-block failure in the clay for both types of experiments. However, the ratio of effective overburden depth against cavity diameter was less than unity.

Similarly, the investigation of the stability of a cemented layer of sand overlying a cylindrical cavity, with and without overburden. The modeling simulated a soil profile

resulting from groundwater extraction in arid regions. The Authors found that the failure of cemented sand layer was steeply occurred along failure planes and formed a truncated conical section. In thicker cemented layer, a compression dome formed however making 25-30% of height of the cavity diameter.

2.4 Studies on Bearing capacity on unsaturated soils

In several scenarios, the foundations are above ground water table with the unsaturated conditions within the soil remaining for the entire lifespan of the foundation. Most studies report the behavior of the foundations subjected to axial loads in unsaturated conditions. Tan et al., (2021), Vo et al., (2016) studied the bearing capacity if strip footings on unsaturated soils using the slip line theory. There studies considered several non-uniform suction profiles corresponding to vertical flow of water by infiltration or evaporation. Their investigations revealed that the influence of the non-uniform suction profile on the bearing capacity is significant, and the depth to the ground water table, the footing width have significant roles in how much suction influences the bearing capacity. Tang et al., (2017) presented an effective stress-based finite element formulation for the computation of the bearing capacities of shallow foundation on unsaturated soils. Using the elastic plastic Mohr-Coulomb model to describe the mechanical behavior of the unsaturated soils, their studies illustrated that the suction profile and hydraulic hysteresis impact directly the bearing capacity of the shallow foundations. In addition, the effects of three drainage conditions such as constant suction, constant moisture content and constant contribution of suction to the effective stress and strength condition were analyzed. Ghasemzadeh et al., (2019) proposed a simple method to predict the bearing capacity of footings placed on unsaturated soil using the limit equilibrium concept. They assumed linear, uniform and nonlinear variations of matric suction distribution. Garakani et al., (2020) investigated the ultimate bearing capacity of shallow foundation through the concept if suction-dependent effective stress. They extended the vesic's equation through an analytical approach considering the influence of matric suction. The other approach used in the study is the unsaturated effective stress state in conjunction with the suction-dependent cohesion through a 3D finite difference code.

Garakani et al., (2020) used water retention for different test materials as key input parameters. The results from their studies showed the dependency of the correction factor introduced to the soil properties, geometrical aspects of the foundation, and its embedding depth. Anand and Sarkar, (2022) developed a novel formulation for allowable bearing capacity of partially saturated geomaterial considering the strength nonlinearity for a steady-state surface flux boundary condition incorporating pseudo-static seismic stresses. The magnitude of surface flux, fluctuation in the water table depth, and horizontal seismic acceleration coefficient on the overall allowable bearing capacity of fly ash deposit. Other researchers focused on the foundation behavior under steady or transient state flow conditions in unsaturated soils. Each research carried out recently on the unsaturated soils have significantly highlighted the variation of the shear strength and the foundation bearing capacity.

Numerous studies have tackled the issues of unsaturated soils, however, to our best knowledge to date, no literature was found investigating the influence of matric suction on the overall stability when the footing-cavity system is encountered. Thus, rigorous studies on the matter are necessary to understand the behavior of the system under such conditions.

Chapter 3. Bearing capacity of a shallow foundation above the soil with a cavity based on Rigid Plastic Finite Element

3.1 Introduction

Underground cavities appear as the results of natural processes and human activities or occasionally as the action of both combined. These actions may cause the ground on which we live to displace. Whether the ground displacements are large and cata-strophic or small and slow, their cumulative impact during the lifetime of humans or civilizations may be large and destructive. Underground cavities either directly damage the built environment and everything constructed by humans or cause it to be more vulnerable to other hazards such as flooding. Around the world, as the demand for land grows and humans increasingly modify their environment, more and more people might be exposed to the instabilities caused by underground cavities (Holzer, 2009). The collapse of the ground into subsurface cavities is a very widespread and potentially damaging phenomenon because of the large depressions (sinkholes) created and its sudden occurrence.

Sinkholes occur due to the erosion of the bedrock or geomaterials around the cavity and can be triggered by rainfall, earthquake, drought, mining, drilling, pumping, tunneling works, etc.(Williams, 2004). Sinkhole activities are commonly the most peculiar hazard in the karst environment Parise et al., 2007; Waltham et al., 2007; Zhou et al., 2008). A karst environment occurs in over 20% of the earth's ice-free continental area, and around 25% of the global population depends on the karst water supply (Ford et al., 2007). The fragility of karst settings, enhanced by human activity, is expected to rise, therefore inducing more sinkholes in the future (Khadka, 2018).

The bearing capacity of a shallow foundation is a non-negligible issue in the geotechnical engineering community. Baus and Wang (1983) conducted an experimental and analytical investigation of the bearing capacity of the footing above void on silty clay using a finite element method considering the soil as an elastic perfectly plastic material. They found that, for each footing, there exists a critical depth below which the presence of a cavity

has a negligible impact on the performance of the footing. Kiyosumi et al., (2011) conducted a series of 1G tests under plane strain conditions on stiff ground with continuous square cavities. The authors revealed three types of failure modes for a single void: bearing failure without void failure, bearing failure with void failure, and void failure without bearing failure. Wu et al., (2020) used an adaptive finite limit analysis (AFELA) code and generalized Hoek–Brown failure criterion to investigate a footing-cavity system with eccentric load in rock masses. Several other studies discussed this complex issue under several assumptions (Ali et al., 2020; Augarde et al., 2003; Badie et al., 1984; Drumm et al., 2009; Wu et al., 2021; Yamamoto et al., 2013). Most of the previous studies have investigated this issue by calculating a stability number N under several different assumptions (Augarde et al., 2003; Keawsawasvong et al., 2019). However, these methods are not straightforward to determine the stability level.

While some studies have touched upon the influence of cavities, mostly focusing on cases where the footing and the cavity are centered, there is a gap in comprehensively addressing how a single cavity with its size and eccentric location to the footing affects the behavior of the Bearing Capacity of the footing. Also, much of the reported research on this subject has been empirical, being associated often with specific locations (Augarde et al., 2003)], making it a reasonable need to provide holistic solutions by incorporating the soil strength parameters. Investigating the impact of the cavity at an offset distance to the footing is crucial in preventing unforeseen hazards to engineering structures or human activities. Therefore, it is necessary to develop for this purpose robust means of risk assessment and effective mitigation strategies for footings in the vicinity of underground cavities. Identifying potential failure modes and quantifying or evaluating stability levels will contribute to devising practical and cost-effective mitigation measures that will be crucial for ensuring the safety and reliability of structures in real-world scenarios. By addressing these issues, significant contributions to advancing the understanding of footing cavity system, refining design practices, and enhancing the resilience of foundations can be achieved.

In this chapter, a parametric study of the influence of the cavity within the cohesive soils and intermediate soils on the bearing capacity of the footing is investigated by employing the Rigid Plastic Finite Element Method. The RPFEM is used in two dimensions under a plane strain condition with an associative flow rule. The investigation of the performance of a shallow foundation above the ground with a cavity considering the variable location and geometry of the cavity is conducted. In addition, the study aims to clarify and establish the influence zone of the cavity on the footing by considering the combination of the geometrical parameters of the cavity and the shear strength of the soils. Finally, a formula that accounts for the shear strength parameters of the soils, as well as the geometry of the cavity, is proposed to predict the stability level. In this study, the terms "cavity" and "void" are used interchangeably.

3.2 Problem definition

3.2.1 Finite element mesh and boundary conditions

Figure 3.1 depicts the typical soil model utilized in this study, featuring the footing and cavity system. In the scenario examined, a shallow foundation with a width denoted as B is placed on the ground with a cavity. The foundation is subjected to uniform vertical loads in homogeneous soil under plane strain conditions. The uniform load is applied to the foundation base, and the foundation is not embedded. The soil characteristics include the cohesion c, the shear resistance angle ϕ, and the unit weight γ. The cavity's shape is square and circular (though it is worth mentioning that the circular configuration is not illustrated here) in the homogeneous soft soil material. To mitigate boundary effects, the model's boundaries are selected to be sufficiently large. The dimensions of the model are specified as a width of 40 m and a height of 18 m. Vertical displacements are exclusively permitted at the lateral boundaries. At the bottom horizontal boundary, displacements in the horizontal and vertical directions are strictly restricted. Two crucial distances are defined in the context of the cavity: h (m), representing the vertical gap between the ground surface and the cavity's center, and D (m), denoting the diameter of the cavity (applicable for a circular cavity as well). Additionally, r (m) is the horizontal distance between the centerlines of the cavity and

the footing. This study assumes that the cavity remains unsupported and statically stable under its self-weight. For enhanced accuracy in the solution, the mesh sizes are deliberately finer around the footing base and the surrounding area. Notably, the cavity's location varies for each analysis case.

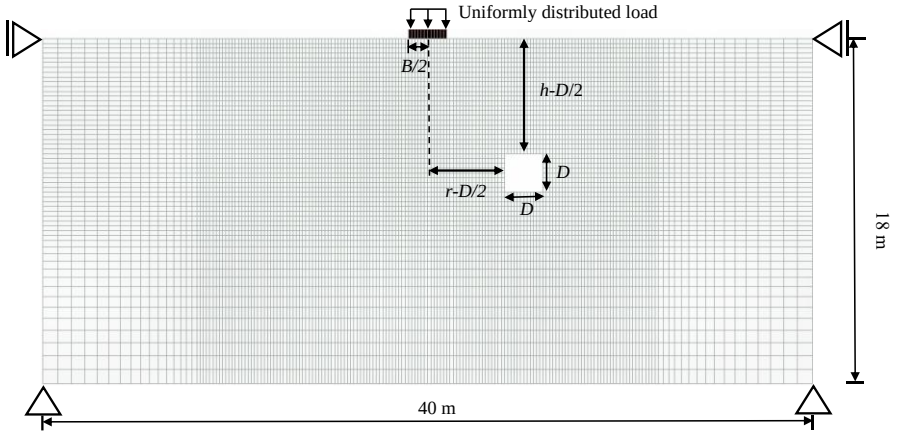

Figure 3.1. Problem definition of a footing laying on the soil with a cavity.

3.2.2 Analysis parameters

The analysis parameters described in Figure 3.1 were varied to evaluate the performance of the footing on the soil with cavity. Table 3.1 shows the different ranges of values on geometry used in the analysis.

The analysis parameters described in Figure 3.1 were varied to evaluate the performance of the footing on the soil with cavity. Table 3.1 shows the different ranges of values on geometry used in the analysis.

Table 3.1. Model geometry.

Parameters	Values
Cavity depth *h-D/2* (m)	2, 4, 6, 8
Cavity diameter *D* (m)	1, 2
Horizontal distance *r* (m)	0, 1, 2, 3, 4, 5, 6, 7, 8, 9, 10
Footing width *B* (m)	1, 2

The parameters listed in Table 3.1 are consistent with those used by Kiyosumi et al.,(2007) who documented void sizes in Japanese uncemented calcareous sediments ranging from less than 1 m to approximately 10 m. Furthermore, numerous studies on cavity-related issues, including those by various authors, have employed cavities within a similar size range as the present study (Badie et al., 1984; Drumm et al., 2009; Kiyosumi et al., 2011). In certain instances, larger values were utilized, with the shear strength parameters of the soils being comparable (Augarde et al., 2003; Baus and Wang, 1983), etc. Consequently, the selected cavity sizes in Table 3.1 are deemed reasonable, aligning with established practices observed in the relevant literature.

Table 3.2 shows the soil properties used in the analysis. The properties considered for the footing are cohesion c = 50,000 kPa and a shear resistance angle ϕ = 0 deg to model a rigid footing. The soil-footing contact is assumed rough.

Table 3.2. Soil parameters.

Properties	Cohesive	Intermediate
Cohesion c (kPa)	10, 50, 75	10, 50
Shear resistance angle ϕ (deg.)	0	10, 20, 30, 40
Unit weight γ (kN/m^3)	16	16

3.3 Outline of the Simulation Method

3.3.1. Rigid Plastic FEM Constitutive Equation

The Rigid Plastic Finite Element Method (RPFEM) was developed by Tamura et al.(Tamura et al., 1984, 1987) and upgraded by (Hoshina et al., (2011) and Nguyen et al., (2016) . The RPFEM calculates the limit load without any assumption of a potential failure mode. The method has been successfully used to examine geotechnical problems (Iqbal et al., 2023; Pham et al., 2023). The RPFEM using the rigid plastic constitutive equation with the Drucker–Prager yield function necessitates only a few soil parameters such as the unit weight, the cohesion, the shear resistance angle, and the dilatancy angle, which is its advantage.

The Drucker–Prager yield function is used in plane strain conditions with an associated flow rule. The Drucker–Prager yield function is expressed as follows:

$$f(\boldsymbol{\sigma}) = \alpha I_1 + \sqrt{J_2} - \kappa = 0 \tag{1}$$

Where, $I_1 = tr(\boldsymbol{\sigma})$ is the first invariant of the stress tensor $\boldsymbol{\sigma}$ and $J_2 = \frac{1}{2}\boldsymbol{S}:\boldsymbol{S}$ is the second invariant of deviator stress tensor **S**. α and κ are soil parameters corresponding to the shear resistance angle and cohesion respectively, and expressed as:

$$\alpha = \frac{\tan\emptyset}{\sqrt{9 + 12\tan^2\emptyset}}, \qquad \kappa = \frac{3c}{\sqrt{9 + 12\tan^2\emptyset}} \tag{2}$$

Where c is the cohesion, ϕ is the shear resistance angle. The volumetric strain rate $\dot{\varepsilon}_v$ for the rigid plastic constitutive equation is expressed as follows:

$$\dot{\varepsilon}_v = tr(\dot{\boldsymbol{\varepsilon}}) = tr\left(\lambda\frac{\partial f(\boldsymbol{\sigma})}{\partial \boldsymbol{\sigma}}\right) = tr\left(\lambda\left(\alpha\boldsymbol{I} + \frac{S}{2\sqrt{J_2}}\right)\right) = \frac{3\alpha}{\sqrt{3\alpha^2 + \frac{1}{2}}}\dot{e} \tag{3}$$

Where λ is the plastic multiplier and $\dot{e}$ is the norm of the strain rate $\dot{\boldsymbol{\varepsilon}}$. $\boldsymbol{I}$ express the unit stress tensors. The strain rate ε, which is purely a plastic component, should satisfy the volumetric constraint condition on the dilation property of the soil as:

$$h(\dot{\boldsymbol{\varepsilon}}) = \dot{\varepsilon}_v - \frac{3\alpha}{\sqrt{3\alpha^2 + \frac{1}{2}}}\dot{e} = \dot{\varepsilon}_v - \eta\dot{e} = 0 \tag{4}$$

Any strain rate which is compatible with the Drucker-Prager yield criterion must satisfy the kinematical constraints of equations Equation (4). η is one coefficient determined by Equation (4) which is one of the dilation characteristics. The dilation constitutive equation is expressed by the Lagrange method after Tamura [26] as follows:

$$\boldsymbol{\sigma} = \frac{\kappa}{\sqrt{3\alpha^2 + \frac{1}{2}}}\frac{\dot{\boldsymbol{\varepsilon}}}{\dot{e}} + \beta\left(\boldsymbol{I} - \eta\frac{\dot{\boldsymbol{\varepsilon}}}{\dot{e}}\right) = 0 \tag{5}$$

The first term expresses the stress component, uniquely determined for the yield function. The second term expresses the indeterminate stress component along with the yield function. The indeterminate parameter β remains unknown until the boundary value problem is solved. Equation (6) introduces the constraint condition on the strain rate into the constitutive equation by using the penalty method.

$$\boldsymbol{\sigma} = \frac{\kappa}{\sqrt{3\alpha^2 + \frac{1}{2}}}\frac{\dot{\boldsymbol{\varepsilon}}}{\dot{e}} + P(\dot{\varepsilon_v} - \eta\dot{e})\left(I - \eta\frac{\dot{\boldsymbol{\varepsilon}}}{\dot{e}}\right) \tag{6}$$

Where P is the penalty constant. This technique makes the computation faster and more stable. It is worth mentioning that the RPFEM is developed based on the upper bound theory of the limit analysis and is effective in the calculation of the bearing capacity of strip footings on all types of soil. The penalty method introduced in the constraint condition is necessary to obtain the collapse load. Since the penalty method incorporates the constraint condition directly into the governing equation, this leads to high computational efficiency. In the simulation, the footing is modeled by the rigid plastic constitutive equation as a rigid material to focus on the plastic behavior of the soils around the footing and the cavity under the vertical loading. Therefore, the elastic modulus and Poisson's ratio are not necessary for this simulation method, and this applies to all types of simulated foundations. A noted property of the method is that in the constitutive equation, the relationship between the stress

and the strain is specified. The norm of strain rate is substantially indeterminate as the focus aims at the limit state of the structure. The stress is determined for the normalized strain rate using its norm to determine the limit load coefficient for the prescribed load. The distribution of the norm of strain in the soil structure indicates the failure pattern. A small norm value indicates a rigid body behavior, however, which cannot be described by the constitutive equation in plastic theory. In the analysis, a threshold value $\dot{e}_o$, small enough to express the rigid body, was introduced and the norm of plastic strain rate e is replaced by $\dot{e}_o$ to avoid dividing any zero in the constitutive equation and thus enable calculation of the rigid body.

3. 3.2. Validation of the Simulation Method

The validation of the simulation method employed in this study was conducted by comparing its outcomes with the findings presented by Baus and Wang, (1983). Figure 3.2 illustrates the comparison between the results of the normalized bearing capacity obtained through RPFEM and those reported by Baus and Wang, (1983). The material properties considered in this analysis include the cohesion c with a value of 65.6 kPa, the shear resistance angle ϕ set at 13.5 degrees, and the unit weight (γ) equal to 18 kN/m^3. The bearing capacity ratio (BC/BC_{NV}), introduced in this study to convey the bearing capacity results, is defined as the ratio of the footing's bearing capacity on soil with a cavity to that on soil without a cavity. While a slight discrepancy is acknowledged, attributed to differences in the constitutive model, a general alignment in the trend of the bearing capacity ratio is evident in both cases, as depicted in Figure 3.2.

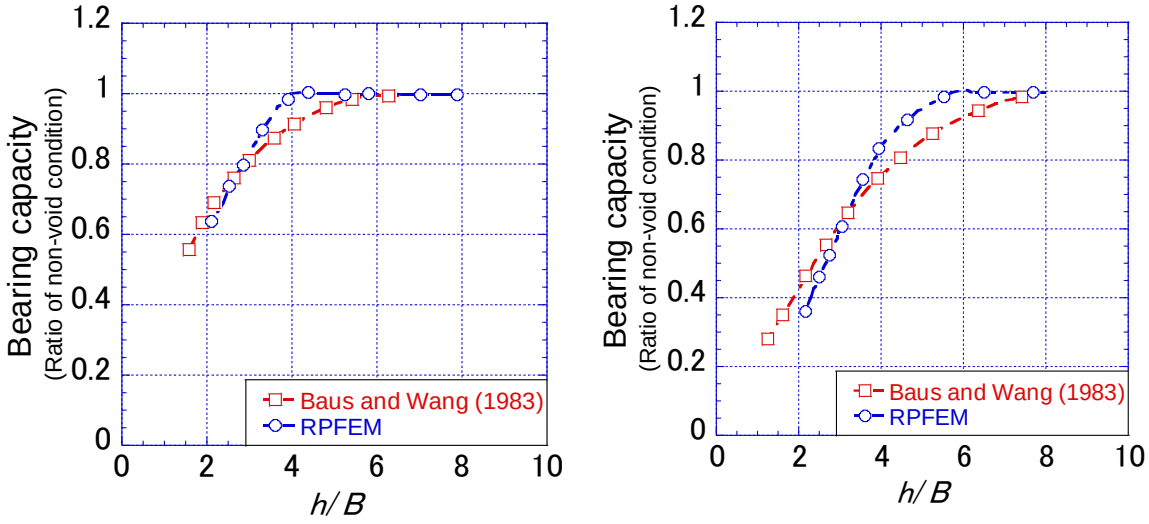

Figure 3.2. Comparison of the variation of the bearing capacity with the depth to cavity obtained by RPFEM and the study by Baus and Wang, (1983) (a) $D/B = 1$; (b) $D/B = 2$.

The comparison yields a noteworthy observation, suggesting a good level of reliability in the simulation method applied in this study. It is important to emphasize that the slight variation in results is primarily linked to distinctions in the constitutive models utilized. Consequently, the overall agreement in the trend of the bearing capacity ratio supports the credibility of the simulation method in this investigation.

3.4 Results and Discussion

The bearing capacity of a shallow foundation on horizontal ground is recognized to be influenced by the soil strength parameters such as the shear resistance angle, the cohesion, the unit weight, and the footing width (Al-Tabbaa A. et al., 1989). In the context of the footing-cavity system, additional factors, including the location, shape, and size of the cavity, come into play and contribute to the variation in bearing capacity. Consequently, this section presents results that elucidate the impact of geometrical parameters on the footing-cavity system. The discussion also delves into the soil's shear strength influence on the bearing capacity ratio (BC/BC_{NV}). It is crucial to emphasize that the unit weight is maintained as

constant for practical considerations throughout this analysis. This approach allows for a focused examination of the specific influence of geometrical parameters on the footing-cavity system and the corresponding bearing capacity, providing valuable insights into the interplay of these factors.

3.4.1 Influence of the geometrical parameters

This section investigates the impact of geometrical parameters on BC/BC_{NV}, utilizing a c-ϕ soil with c = 10 kPa and ϕ = 30 degrees for analysis. Figure 3.3a presents the influence of footing width B on BC/BC_{NV}, revealing a decreasing trend along the distance r/D as the footing width changes from 1 m to 2 m. The most significant difference is noted at r/D = 0, gradually diminishing at distant locations. Figure 3.3b illustrates the difference in BC/BC_{NV} resulting from cavity shape, with a notably higher value observed for a circular cavity. The smooth stress distribution around the circular cavity leads to a less pronounced impact on the bearing capacity compared to cases with square cavities. Kuwano, (2021) highlighted a substantial decrease in the bearing capacity of a footing above square or rectangular cavities. Additionally, Figure 3.3b emphasizes the substantial difference in BC/BC_{NV} values when the cavity is directly beneath the footing (r/D = 0) and as it progressively shifts to normalized horizontal distances r/D.

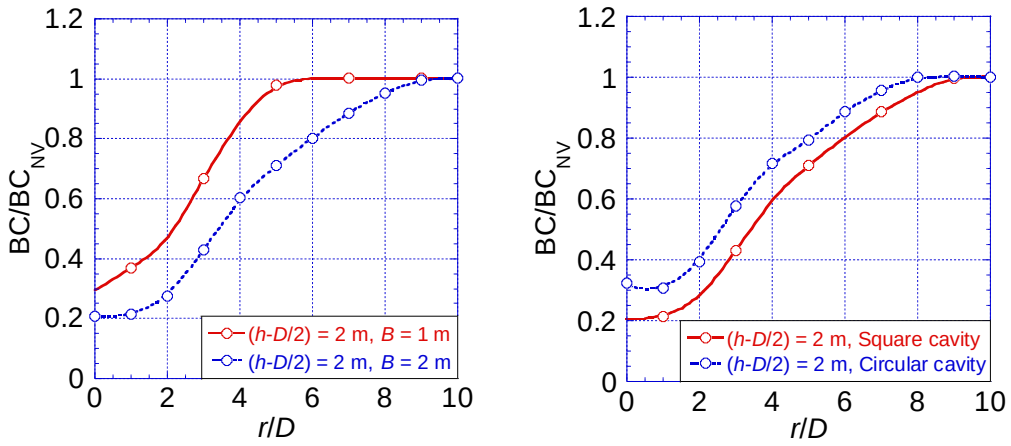

(**a**) (**b**)

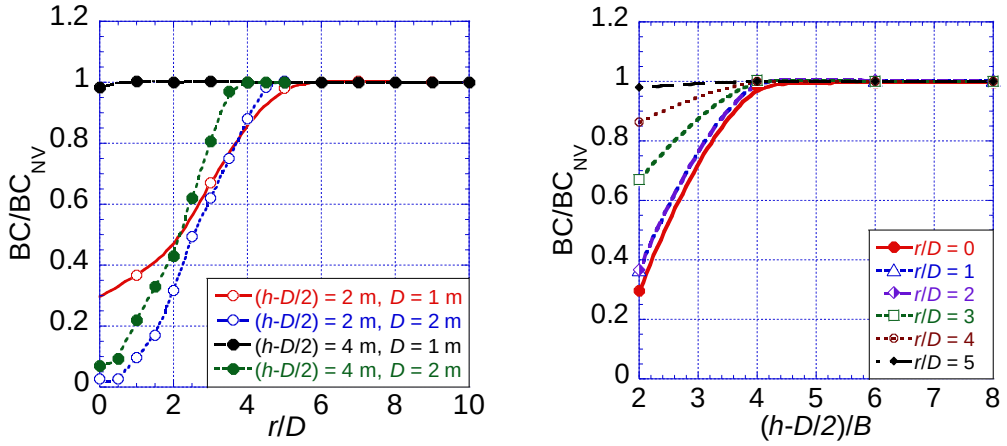

(**c**) (**d**)

Figure 3.3. Effects of different geometrical parameters on the normalized bearing capacity BC/BC_{NV}. (**a**) Footing width (for cases B = 1, 2 m; D = 1 m); (**b**) cavity shape (for cases B = 2 m; D = 1 m); (**c**) cavity size (for cases B = 1 m, D = 1, 2 m); (**d**) cavity depth (in case B = 1m).

In Figure 3.3c, the influence of cavity diameter D on BC/BC_{NV} is explored, revealing noticeable variations with increased D. Figure 3.3d depicts the effects of cavity depth normalized to footing width B as $(h\text{-}D/2)/B$ on BC/BC_{NV}. Within the range $(h\text{-}D/2)/B$ = 2 to $(h\text{-}D/2)/B$ = 4, significant BC/BC_{NV} variations are evident for various normalized horizontal distance values (r/D). Smaller r/D values correspond to steeper slopes between $(h\text{-}D/2)/B$ = 2–4. In summary, the considered parameters collectively exert a noticeable impact on Bearing Capacity behavior. Notably, when the cavity is sufficiently distant from the footing, BC/BC_{NV} tends toward 1, indicating the presence of a critical line that elucidates an influence zone.

3.4.2 Influence of the soil strengths on the BC/BC_{NV} of the footing-cavity system

3.4.2.1 Normalization

The analysis of the bearing capacity under several conditions considering different geometrical parameters and soil types (cohesive soils, intermediate soils) is investigated. This study elucidates the correlation of the influence zone by introducing a novel normalization concept based on the boundaries of the footing's failure surface. These boundaries are

established in both horizontal and vertical directions within the ground without cavity, as depicted in Figure 3.4. The failure surface beneath the footing is conceptualized with three zones, as documented in the literature (Al-Tabbaa A. et al., 1989; Lee et al., 2014), specifically applicable to homogeneous soil subjected to vertical loading. The lateral expansion of the failure domain primarily depends on the shear resistance angle.

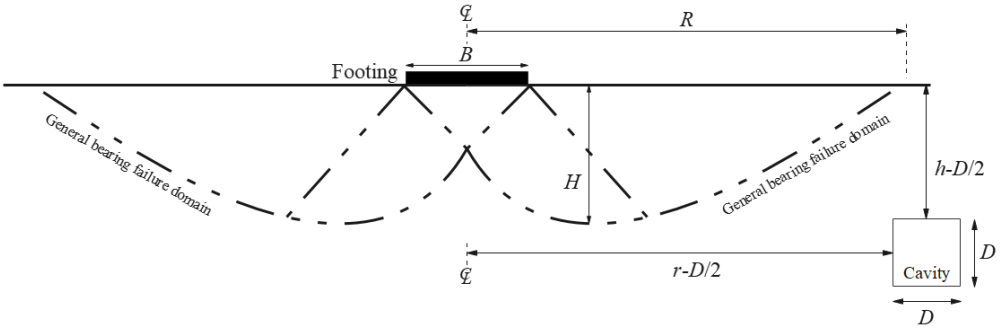

Figure 3.4. General bearing failure pattern with the normalization parameters.

The newly introduced normalization parameters are the dimensions *R* and *H*. Table 3.3 shows the parameters *R* and *H* for the various types of ground without the cavity obtained by the RPFEM results. It is worth noting that these values are empirically obtained from the results of simulation with RPFEM on deformation analysis of footing on the soil without voids (Figure 3.5). As a reference, empirical determination of the plastic mechanism or failure surface has been used to determine failure domains in the case of total and effective stress analyses (Tamura, 1990; Zhou et al., 2018).

These parameters exert significant influence by governing the development of the failure mode in the footing-cavity system. When the cavity lies outside the failure domain, i.e., when (*r*-*D*/2) > *R* and (*h*-*D*/2) > *H*, its impact on the footing's performance diminishes with increasing distances of (*r*-*D*/2) and (*h*-*D*/2). Conversely, critical failure modes emerge when the cavity is situated within the footing's failure domain. Consequently, the results are presented as the distribution of BC/BC_{NV} within the plane of normalized distances, with (*r*-*D*/2)/*R* representing the X-axis and (h-D/2)/*H* for the *Y*-axis, respectively.

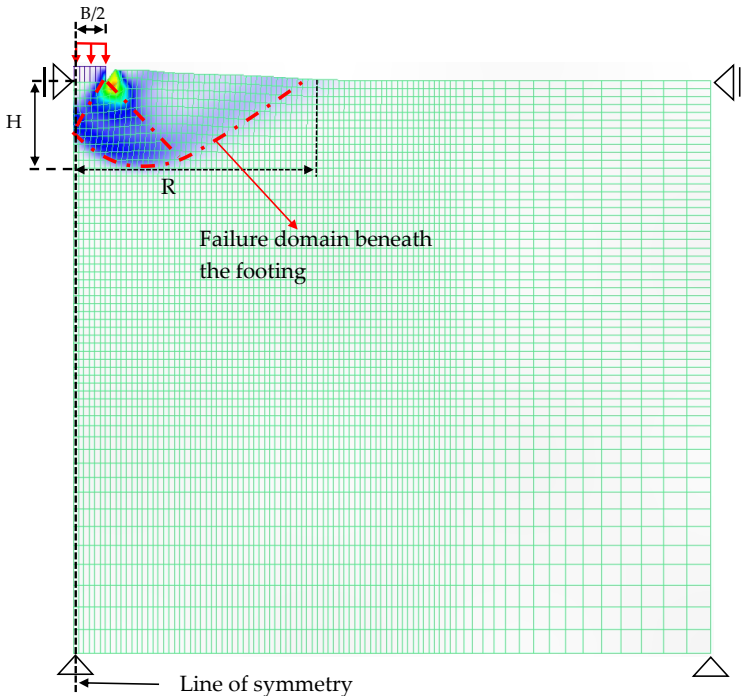

Figure 3-5. Illustration of the obtention of parameters *R* and *H* on the RPFEM deformed model of the footing on the soil without cavity.

Table 3.3. (**a**) Normalization parameters *R* and *H* obtained with the RPFEM results. Cohesive soils. (**b**) Normalization parameters *R* and *H* obtained with the RPFEM results. Intermediate soils with small cohesion soils. (**c**) Normalization parameters *R* and *H* obtained with the RPFEM results. Intermediate soils with large cohesion soils.

Cohesion *c* (kPa)	***ϕ* (deg)**	***B* (m)**	***R* (m)**	***H* (m)**
		(**a**)		
50	0	1	2.5	1.5
	0	2	4.5	2.25
		(**b**)		
10	10	1	3.5	1.5
		2	5.5	3
	20	1	4	1.5
		2	6	3
	30	1	4.5	1.75
		2	7.5	2.75
	40	1	7.5	2.25
		2	7.5	2.5
		(**c**)		
50	10	1	3.5	1.5
		2	5.5	2.75
	20	1	4	1.75
		2	7	3
	30	1	4.5	2.25
		2	8.5	3.25
	40	1	7.5	2.5
		2	12	4.5

The space (*X*, *Y*) is divided into two primary regions, distinguished by BC/BC_{NV} values below 1 and equal to 1, with the critical line serving as the demarcation between these areas. The

region corresponding to BC/BC_{NV} equal to 1, indicated in grey in the figures, is referred to as a stable zone or a no-influence zone. This designation signifies that, within this area, the presence of the cavity has a negligible impact on the performance of the footing. It is important to note that, due to numerical errors, the boundary between these two main zones is occasionally set at 0.98 or 0.99 throughout this paper.

3.4.2.2 Influence of the Cohesive Soil Materials

The analysis of BC/BC_{NV} for the footing-cavity system is conducted in cases involving cohesive soils. Figure 3.6a shows the variation of BC/BC_{NV} with r/D for a cohesive soil material (c = 10 kPa). The results exhibit a single line, visible only for the scenario of a shallow cavity within the range r/D = 4 to r/D = 10. It is noteworthy that the value of BC/BCNV barely reaches unity along the horizontal axis. This is attributed to the dominance of shear stress induced by the soil unit weight around the cavity over cohesive resistant forces. In particular, the range between r/D = 0 and r/D = 4 is an initially unstable area and is out of the target of this study. Figure 3-6b–d shows the failure mechanism for a cavity at the points K, L, and M, respectively. The strain distributions reveal a general shear failure at the footing base and roof failure at the cavity with an extension of relatively small strain between the footing and the cavity. In addition, the closer the footing and cavity are, the stronger the interaction inducing the void and bearing failure (Figure 3.6b, c).

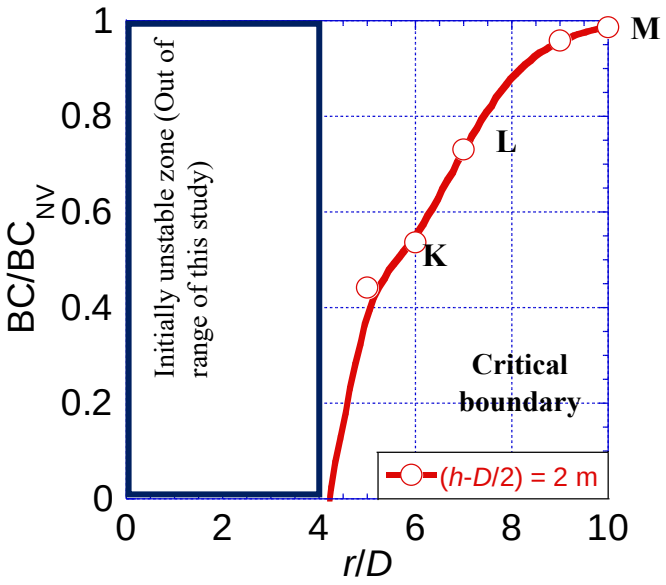

(a) Variation of BC/BC_{NV} along r/D

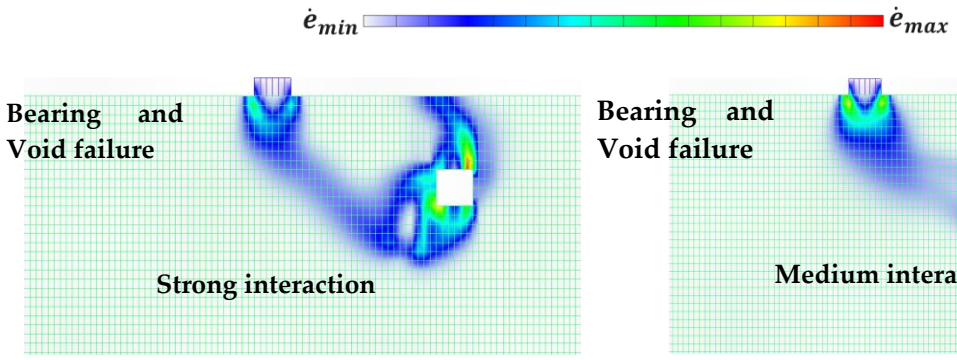

(b) Point K (r/D = 5)

(c) Point L (r/D = 7)

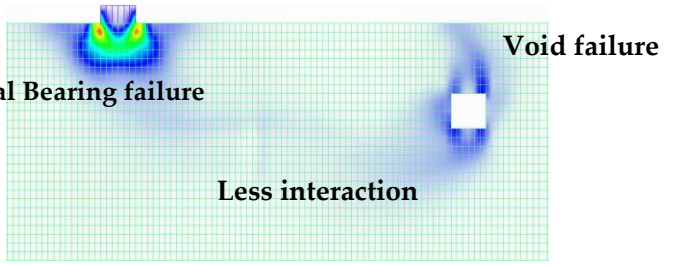

(d) Point M (r/D = 10)

Figure 3-6. Behavior of the BC/BC_{NV} variations along r/D and the failure modes for cohesive soils with small cohesion (c = 10 kPa). (**a**) Variation of BC/BC_{NV} along r/D; (**b**) Point K (r/D = 5); (**c**) Point L (r/D = 7); (**d**) Point M (r/D = 10).

Figure 3.7 illustrates the distribution of normalized BC/BC_{NV} within the plane defined by normalized distances X and Y when soil cohesion c is set at 50 kPa. This representative result corresponds to a footing size of B = 1 m and a cavity size of D = 1 m. The findings reveal that BC/BC_{NV} increases with the augmentation of both X and Y. The BC/BC_{NV} varies within the range of 0.80 to 0.99 (approximately 1). It is also observed that the influence of the cavity in this type of soil is 3 times more emphasized in the vertical direction than in the horizontal direction. This is because, for the cohesive soils, the slip surface beneath the footing is not expanding widely in the horizontal direction. The passive earth pressure at the rigid wedge directly beneath the footing is decreased due to the presence of the void.

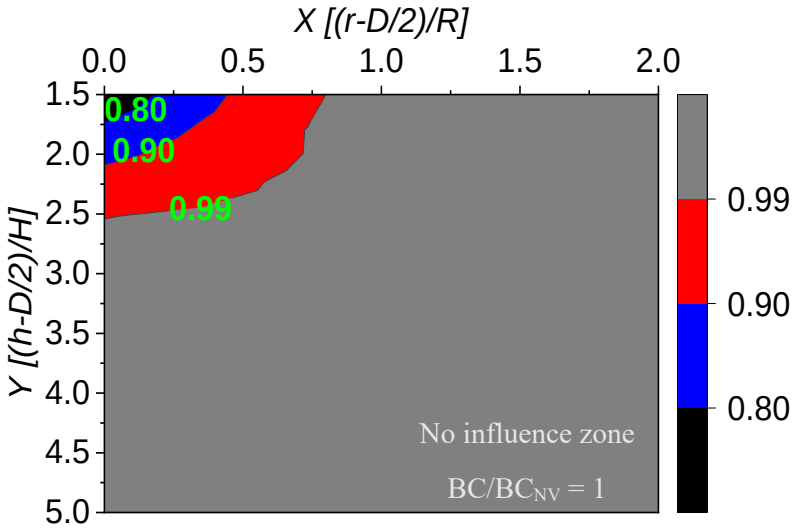

Figure 3.7. Distribution of the BC/BC_{NV} within the X and Y direction for the cohesive soils (c = 50 kPa).

3.4.2.3 Influence of the intermediate soil material

The intermediate soil types were differentiated based on variations in cohesion c and shear resistance angle ϕ. These categories include soil with low cohesion and low shear resistance angle ϕ, soil with low c and high ϕ, soil with high c and low ϕ, and soil with high c and high ϕ. In Figure 3.8a, the BC/BC_{NV} variation is depicted within a soil characterized by low cohesion (c = 10 kPa) and a low shear resistance angle (ϕ = 20 deg). The influence zone, where the ratio BC/BC_{NV} is less than 1, remarkably expands in the vertical direction. This expansion is attributed to the low shear resistance angle, causing the soil to exhibit cohesive-like behavior. Furthermore, a small area, highlighted in black (BC/BC_{NV} = 0.3), indicates a more significant influence than observed in other cases, as it falls below the allowable BC with a factor of safety of 3. Figure 3-8b illustrates the distribution of BC/BC_{NV} when the shear resistance of the previous c-ϕ soil is increased to ϕ = 30 deg. The trend in the footing's performance with the cavity's location remains consistent with the previous case. However, the expansion in the Y direction is comparatively reduced compared to the scenario in Figure 8a, and an area showing BC/BC_{NV} less than the allowable BC is not observed.

Figure 3.8c, d presents the distribution of BC/BC_{NV} with distances X and Y for a c-ϕ soil with high cohesion (c = 50 kPa) and low shear resistance angle (ϕ = 20 deg), and high shear resistance angle (ϕ = 30 deg), respectively. In comparison to the preceding cases (Figure 3-8a, b), the influence zone notably contracts in both directions. This contraction implies that a cavity in soil with substantial shear strength is more stable, and the potential to collapse is reduced compared to scenarios involving soil with lower shear strength.

Overall, the influence zone due to the presence of the cavity on the footing exhibits high sensitivity in the vertical direction and low sensitivity in the horizontal direction, particularly evident in soils with smaller shear resistance angles. It is important to highlight that the influence zone in the horizontal direction does not exceed $X = 1$. The denominator R, integral to the calculation, depends on the shear resistance angle and the dilatancy angle (equivalent to ϕ, given the use of the associated flow rule). A higher dilatancy angle results in a larger R. Consequently, under these conditions, significant expansion of the influence zone in the horizontal direction is limited. Similar considerations apply to the vertical direction, where the variation of H is less pronounced than that of R due to the increasing confining stress with depth, thus explaining the observed sensitivity in the vertical direction.

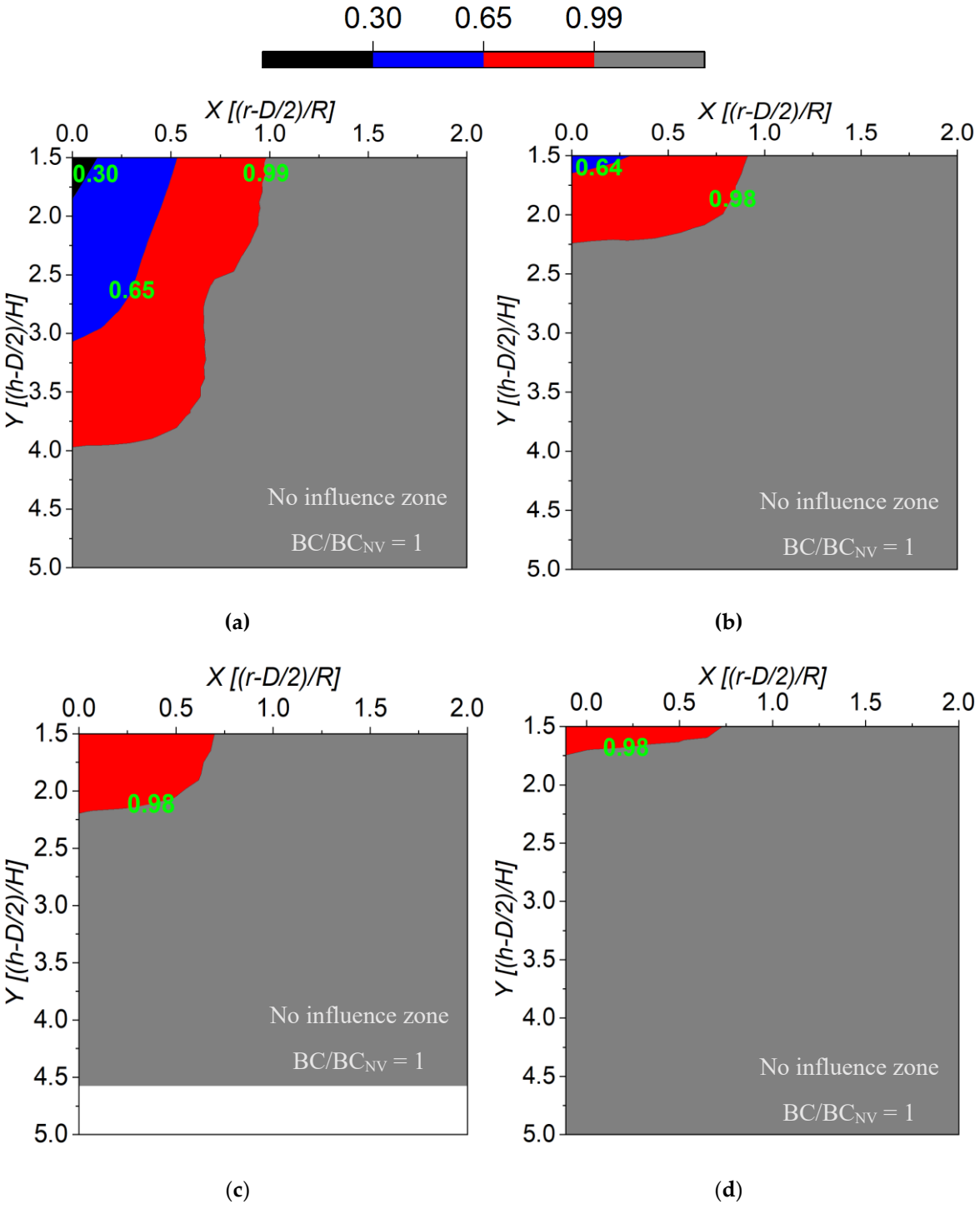

Figure 3-8. Distributions of the BC/BCNV within the X and Y directions for the intermediate soils. (**a**) c = 10 kPa, ϕ = 20 deg; (**b**) c = 10 kPa, ϕ = 30 deg; (**c**) c = 50 kPa, ϕ = 20 deg; (**d**) c = 50 kPa, ϕ = 30 deg.

3.4.3 Failure mode

This section displays some failure modes observed within the soil (c-ϕ soils) at some selected locations of the cavity (r = 1 m, 5 m, and 10 m with the cavity size D = 2 m) considering the same geometrical settings for different shear strength parameters. The general deformed models revealed the existence of 2 main failure modes. The Bearing failure where the plastic domain expands only beneath the footing. This failure mode is similar to the condition where there is no cavity within the soil—then, the Bearing and Void failure. This is a combined failure due to the cavity and footing interaction where the plastic domain expands between the underneath of the footing and the vicinity of the cavity. The strain rate concentrates at the footing base as well as the cavity's edge. The interaction is dependent on the range of distance between the footing and the cavity. So, the interaction ranges from less, medium, or strong interaction regarding the strain rate (see Figure 3.6). The void failure, where the plastic domain is located mainly at the cavity edges and roof, portrays a possibility of collapse due to the soil's self-weight. This latter, however, is out of the range of this study. The results show at least the bearing failure as being triggered by the loading conditions and occurs mostly at the shallowest depths.

Figure 3.9a, b displays the failure modes for the cavity located at the depth (h-D/2) = 8 m and the horizontal distance r = 1 m. The condition case in Figure 3-9a (Bearing and Void failure) shows that the strain rate is also concentrated at the cavity wall (lower parts). The farther the cavity exists horizontally, the less the interaction between the footing and the cavity occurs. Figure 3-9b shows that for the identical geometrical conditions with Figure 9a, a change of the failure mode in the case only ϕ is higher is observed. The change of failure to the Bearing failure is remarkable as opposed to Figure 3-9a. This is due largely to the value of H of the failure domain generated considering this typical shear strength. The failure mechanisms are in agreement with those obtained by Wu et al., (2021) who discussed the bearing capacity and failure mechanism of a rough strip footing located above the cavity by introducing a method that considers random and complex shapes based on an Inverse Discrete Fourier Transform (IDFT).

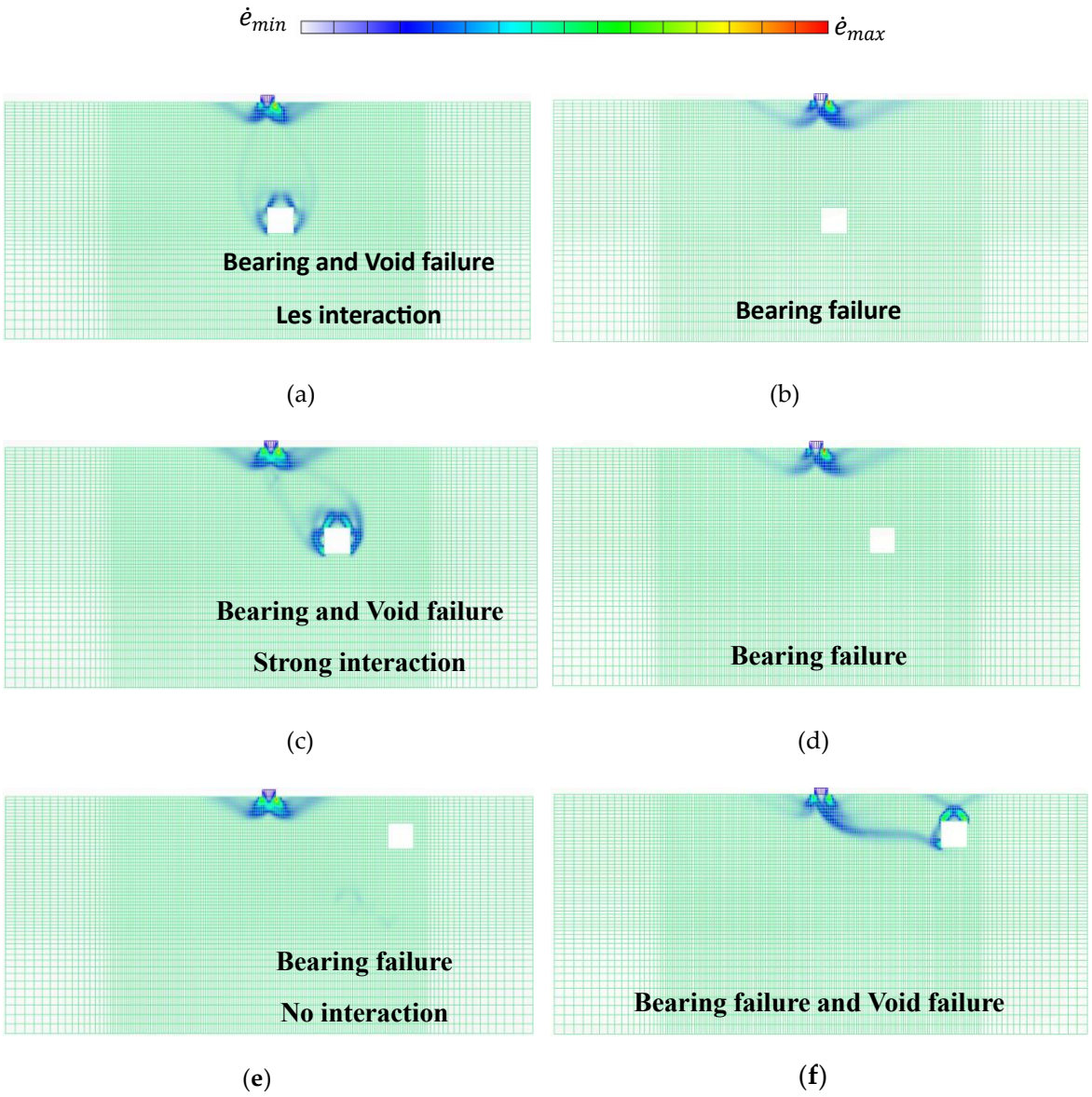

Figure 3.9. Failure modes for different shear strength parameters c = 10 kPa, ϕ = 30 deg (left) and c = 10 kPa, ϕ = 40 deg (right). (**a**) B = 1 m, D = 2 m, r = 1 m, h-D/2 = 8 m; (**b**) B = 1 m, D = 2 m, r = 1 m, h-D/2 = 8 m; (**c**) B = 1 m, D = 2 m, r = 5 m, h-D/2 = 6 m; (**d**) B = 1 m, D = 2 m, r = 5 m, h-D/2 = 6 m; (**e**) B = 1 m, D = 2 m, r = 10 m, h-D/2 = 2 m; (*f*) B = 1 m, D = 2 m, r = 10 m, h-D/2 = 2 m.

In Figure 3.9c, d, with the cavity located at r = 5 m, h-D/2 = 6m, the Bearing and Void failure is observed for the case ϕ = 30 deg (Figure 3.9c). The footing and the cavity strongly interact, and the failure domain around the cavity portrays a high strain rate. However, when ϕ is higher (ϕ = 40 deg), the failure mode is drastically changed (Figure 3.9d) to the Bearing failure, similar to Figure 3.9b. Figure 3.9b, d reveals that for large shear resistance angles, the influence of the cavity in deeper layers is not significant on the performance of the footing. Figure 3-9e, f, with the cavity located at r = 10 m, h-D/2 = 2 m, an interesting observation of the failure changes against the shear resistance angle reveals that for the low shear resistance angle ϕ = 30 deg; the influence of the cavity on the footing at shallow depths is ceased at large distance r. This is supported by the only Bearing failure observed in Figure 3-9e. However, for the case with a large shear resistance angle ϕ = 30 deg, the strong interaction of the footing-cavity system is observed. Briefly, the analyses of the typical failure modes revealed an interesting role of the shear resistance of the soil on the overall stability and expansion of the influence zone of the cavity. It was found that, for the small ϕ, the void failure is accentuated in deep layers while, for the large ϕ, due to the large shear band generated (large R), the void failure occurs mainly for the shallow depths of the cavity and cavity in deep layers do not influence the footing performance (Bearing failure).

3.4.4 Influence Zone and Critical Boundary Equations

The BC/BC_{NV} distribution within the space (X, Y) of the different soil materials is shown in Figures 3.7 and 3.8 produced the critical line shown in Figures 3.10 and 3.11. From these figures, the critical lines are approximately expressed as:

$$Y = pX^2 + q \qquad (7)$$

where X = (r-D/2)/R and Y = (h-D/2)/H. The coefficients p and q are varied depending on the shear strength parameters and the conditions of the soils.

The BC/BC_{NV} in the case of square cavities is the lowest compared with the circular cavities. Therefore, Equation (7) is established based on the square cavities meaning, the

worst scenario in terms of the cavity geometry, and can be safely applied to other shapes of the cavity such as circular or oval-shaped cavities.

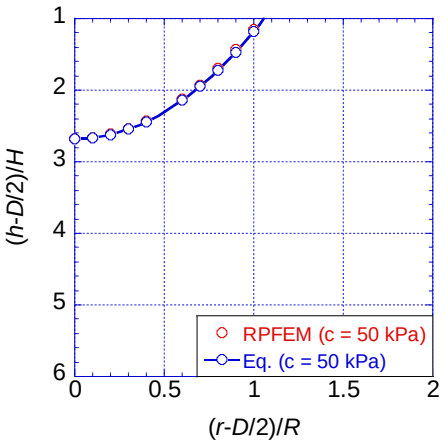

Figure 3-10. Critical line in cohesive soil (c = 50 kPa).

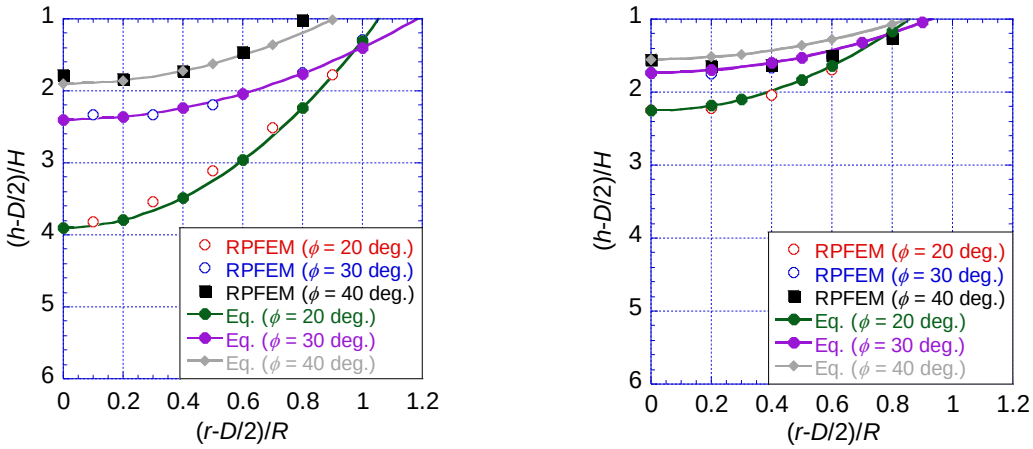

(a) (b)

Figure 3-11. Critical lines for the intermediate soils with variable ϕ (a) c = 10 kPa; (b) c = 50 kPa.

3.4.4.1 Influence Zone in the Cohesive Soils

The coefficients p and q for the cohesive soils are shown in Table 3.4. Figure 3.10 shows the critical lines for the cohesive soils based on the RPFEM results and the proposed Equation

(7) using the coefficient shown in Table 3.4. It shows a good agreement. It can be expressed from Figure 3-10 that the influence zone is deeply expanded in the vertical direction.

Table 3.4. Coefficients p and q for cohesive soils.

Coefficients	Values
p	−1.5
q	2.68

3.4.4.2 Influence Zone in the Intermediate Soils

The coefficients p and q for the intermediate soils are shown in Table 3-5. Figure 3-11 shows the critical lines for intermediate soils based on the RPFEM results and the proposed Equation (7) using the coefficient shown in Table 3-5. It shows a good enough agreement and evaluates the critical lines on the safe side although a small discrepancy is observed. It can be expressed from the comparison of these coefficients that the influence zone is influenced more by the cohesions and less by the shear resistance angle.

Table 3.5. Coefficients p and q for intermediate soils.

Coefficients	Values
p	$a_0 \tan\phi \left(\frac{a_1}{a_0} + \frac{a_2}{a_0}\tan\phi + \cot\phi\right)$
q	$b_0 \tan\phi \left(\frac{b_1}{b_0} + \frac{b_2}{b_0}\tan\phi + \cot\phi\right)$
a_0	$-10.37 + 1.94 \times \left(\frac{c}{\gamma B}\right)$
a_1	$28.51 - 6.04 \times \left(\frac{c}{\gamma B}\right)$
a_2	$-21.47 + 4.82 \times \left(\frac{c}{\gamma B}\right)$
b_0	$10.57 - 2.34 \times \left(\frac{c}{\gamma B}\right)$
b_1	$-22.29 + 5.98 \times \left(\frac{c}{\gamma B}\right)$
b_2	$14.16 - 3.94 \times \left(\frac{c}{\gamma B}\right)$

Based on the above discussion, the RPFEM-obtained solutions can help determine the influence zone of the cavity on the BC/BC_{NV} of the footing resting on various types of soils, depending on the shear strength. In addition, it is possible to determine the necessary depth and radius to investigate the presence of the cavity in practical engineering and it also helps to predict the failure mechanism of the footing-cavity system.

3.4.5 Discussion

In the preceding sections, results were sequentially presented, exploring the impact of geometrical parameters on the bearing capacity behavior of the footing in the presence of a cavity. Additionally, an examination of the influence of soil strength parameters was undertaken, specifically focusing on cohesive and intermediate soil types. Furthermore, a detailed analysis of typical failure mechanisms was conducted to comprehend variations in stability levels under various conditions. These analyses have contributed to the formulation of proposed solutions aimed at determining the critical boundary of the zone of influence of the cavity on the bearing capacity.

The analysis of geometrical parameters, as depicted in Figure 3.9, demonstrates that an increase in the footing width B leads to a reduction in the normalized bearing capacity BC/BC_{NV}. This trend is attributed to the heightened footing pressure magnitude, which intensifies the plastic mechanism and deformations, as illustrated in Figure 3-4. Consequently, a larger footing width is susceptible to the influence of nearby cavities, as highlighted in previous research (Kiyosumi et al., 2011). Furthermore, the cavity shape analysis indicates that square cavities yield lower BC/BC_{NV} values compared to circular cavities. The circular shape facilitates a smoother stress distribution within the soil, while square cavities result in an expanded stress distribution at the cavity edges. Additionally, the cavity's proximity to the centerlines of the footing is revealed to exert the most significant in-fluence on bearing capacity. At greater depths or horizontal distances, this influence diminishes, and the bearing capacity tends to recover to values similar to scenarios without a cavity. These findings align with prior studies by various researchers (Kiyosumi et al., 2007., 2011). However, it is noteworthy that Al-Tabbaa et al., (1989). reported negligible influence on bearing capacity

concerning cavity shape. Consequently, our solution design is based on square cavities, representing severe scenarios and providing a conservative approach to ensure safety.

The exploration of soil strength parameters in cohesive and intermediate soils underscores the significance of studying this issue across a diverse range of soil types rather than in localized regions. The introduction of normalized parameters, derived from the plastic mechanism of the footing without a cavity, serves to quantify and establish a well-defined distribution of BC/BC_{NV} within the plane (X, Y) based on geometrical parameters. Cohesive soil cases, within the considered range of cohesion, demonstrate that the bearing capacity is notably affected by cavities beneath the footing, particularly those close to the centerline of the footing. Conversely, in intermediate soils, the distribution of BC/BC_{NV} within the plane (X, Y) is influenced by the combination of cohesion c and shear resistance angle ϕ. Low cohesion and low shear resistance angle soil types pre-dominantly impact the vertical direction (Y), with a larger influence zone compared to cases with higher shear resistance angles. For the latter, the influence decreases in the vertical direction, while in the horizontal direction (X), an impact is observed, especially for shallow cavities at large X (Figure 3.9a, b). In fact, the slip surface is widened due to its large dilatancy angle as the associated flow rule is assumed; therefore, strain rate expands more horizontally. However, the BC/BC_{NV} varies between 0.30 and 0.98 (approx. 1). As the bearing capacity is above the allowable BC at $BC/BC_{NV} = 0.3$, it can be expected that in this range less impact on the footing occurs. The cases of intermediate soils with high cohesion with variable ϕ (Figure 3.9 c, d) showed the BC/BC_{NV} = 0.65–0.98 with a larger influence zone when ϕ is low. For this last case, as previously, these results also revealed that ϕ, consequently the dilation angle controls the direction of the zone influence. However, within the soils with larger strengths, the influence of the cavity is mostly at shallow depths.

In deep depths, soils with larger strengths exhibit reduced influence of the cavity due to the nonlinear increase of shear strength with ϕ as a function of depth. The observed results align with findings by Zhou et al., (2018) who investigated strip footing bearing capacity on c-ϕ soils with square voids. Comparative results of normalized bearing capacity factors

(BC/BC_{NV}) with studies by Zhou et al., 2009); Kiyosumi et al., (2011); Lee et al., (2019) illustrate agreement with results obtained from RPFEM (Figure 3-12).

The failure mechanisms observed in cavities with horizontal gaps from footing centerlines delineate two types of failures, emphasizing the significance of soil shear resistance in predicting failure mechanisms. Bearing failure occurs when cavities are sufficiently distant from the footing centerline and outside the slip surface. On the contrary, bearing and void failure result in rupture lines developing from the edges of the footing to cavity walls and roof, potentially inducing differential settlements over a broader area.

While Zhou et al., (2009) confirmed similar behavior, their proposed solution lacks a formula for evaluating stability levels. In contrast, based on RPFEM results, this study proposes an equation for the critical boundary, incorporating normalized parameters *R* and *H*, cavity dimensions, and soil strength. This solution confidently predicts the influence zone based on normalized parameters. In summary, RPFEM demonstrates robustness in analyzing the studied issue, encompassing both bearing capacity and stability concerns.

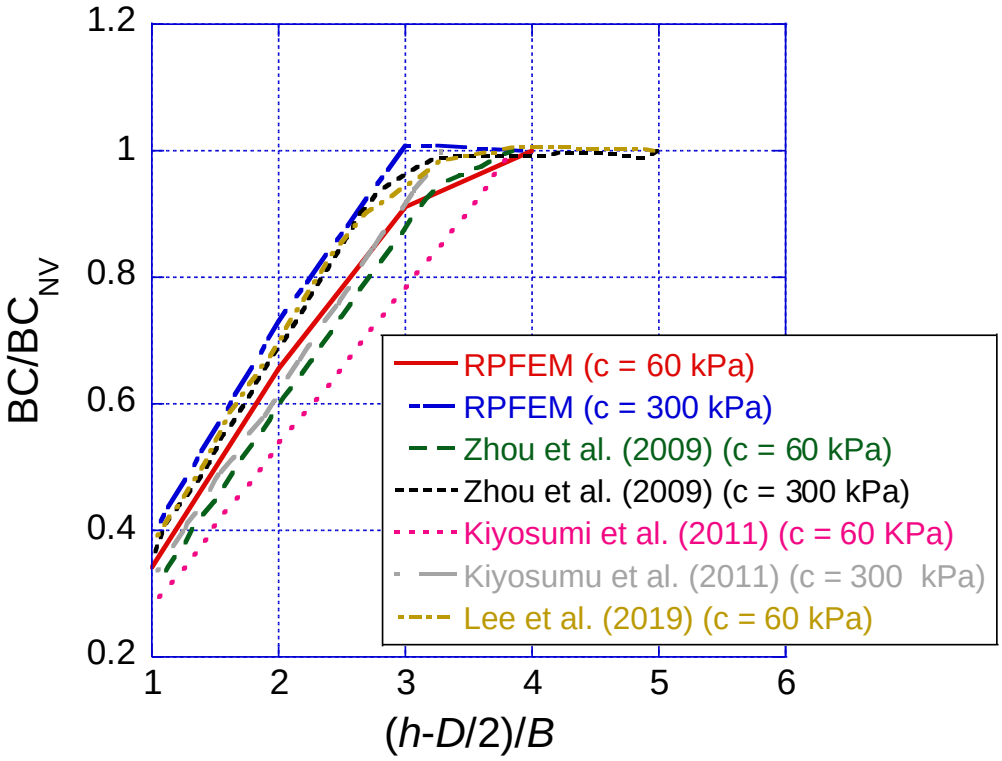

Figure 3.12. Comparison between BC/BC_{NV} derived from RPFEM and that of previous studies (Zhou et al., 2009; Kiyosumi et al., 2011; Lee et al., 2019) (c = 60 kPa and c = 300 kPa).

3.4.6 Example of Engineering Application of the Charts of Influence Zone

For the case study by Yan et al., (2009) an application of the critical line's equation is demonstrated. The study concerned a region in China named Liangshuijing. In the project area, the soil consists of light yellow and hard plastic-like red clay with an average thickness of 9.6 m, and the bedrock mainly consists of light grey, thin-layered, and moderately weathered limestone. The 2.0 m × 2.0 m independent foundation under the column was adopted in the project. The basis depth is 2.0 m, the clay weight γ = 18.2 kN/m^3, c = 53 kPa, ϕ = 28 deg. There is an oval cavity with a semi-major axis of 0.3 m and a short half-axis of 0.25 m under 5.0 m of foundation. There are no fillings in the cavity. Based on these data,

we introduce a case of utilization of the critical lines with a dry condition to determine stability.

Assuming that the cavity's centerline coincides with the footing centerline (Figure 3.13), the coefficients q in Table 3.5 is determined using b_0 = 7.16; b_1 = -13.58; b_2 = 8.42 based on the shear strength parameters shown above. As a result, the calculated critical boundary is Y_{cri} = 2.29 where X = 0. The stability condition is expressed by comparing the (h-D/2)/H = 1.26 obtained from the provided geometrical conditions (h = 5 m, D = 0.5 m, and H = 3.25 m) to the critical value Y_{cri} of 2.29. This comparison shows that the cavity is involved within the unstable zone and agrees with the results by Yan et al., (2009), who estimated an unstable condition based on their calculated stability factor such as 0.982 < 1.0. Even though the comparison with our method is indirect, it can reach a similar conclusion about the state of stability, which is one of our objectives.

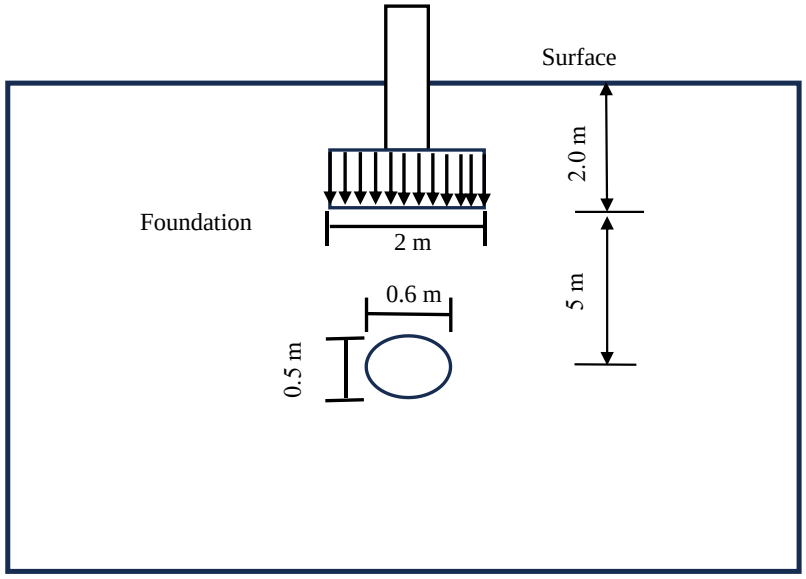

Figure 3.13. Illustration of the model of the footing-cavity system by Yan et al. 2009.

3.5 Limitations

It is noteworthy to mention that the study focuses on the bearing capacity of the footing above square and circular cavities. However, since the results of the square cavities represent a worse scenario, our solution is built based on the results of the square cavities, and thus fewer results of the circular cases were shown. In addition, some researchers confirmed that the shape of the cavity has negligible influence on the bearing capacity characteristic (Baus and Wang, 1983; Lee and Kim, 2019). This study is limited to the cases where the soil strengths, especially, are not as large as in rock-like materials. This means that, in the case of a material strength higher than 100 kPa, the solution may not be sufficient. In addition, the cavity size should be within the range of the parameters used in the present study to provide a realistic solution. This being said, future research can focus on much larger cavity sizes and stronger geomaterials. Other aspects in which clarifications are needed should consider the cases of non-homogenous soil materials (layered ground), foundation load inclinations, and most interestingly an examination of the water table level and drainage conditions as the changes in groundwater levels can affect soil properties and the behavior of the footing-cavity system.

In light of our comprehensive study on the influence of cavities on the bearing capacity of footings, we propose a set of recommendations for incorporation into construction practices and codes. It is imperative that construction practitioners and regulatory bodies recognize the potential impact of subsurface voids on the stability of foundations. Our findings underscore the need for applying a straightforward formula to assess the stability level when a cavity is discovered. We suggest the integration that the formula be integrated into the use of real case projects so that it can be improved if necessary. Furthermore, we recommend the development of guidelines within construction codes to address the stability concerns associated with cavities, including specific design methodologies and safety factors. Emphasizing the importance of proactive cavity detection and mitigation measures in construction regulations will contribute to enhanced structural stability and, ultimately, safer built environments. Continuous collaboration between geotechnical engineers, construction professionals, and regulatory authorities is crucial to ensuring the effective implementation of these recommendations in construction practices.

3.6 Conclusions

The investigations yielded the following outcomes.

(1) The RPFEM produced reasonable results of the bearing capacity with a cavity for the highly cohesive soils and the intermediate soils except in the cases where their cohesion and shear resistance angle were low.

(2) The bearing capacity is influenced by the footing width, the location of the cavity, as well as the shape. The combination of these geometric parameters with the shear strength parameters of the soils provided an understanding of the distribution of the BC/BC_{NV} in the horizontal and vertical direction to clarify the influence zone of the cavity.

(3) The influence zone is dependent on the shear resistance parameters. By normalizing the influence zone based on the general bearing failure domain parameters in the intact ground, it is found that the influence zone has a great sensitivity in the vertical direction

but less in the horizontal direction. It is influenced more by the cohesions and less by the shear resistance angle.

(4) The equation of the critical equation is proposed to distinguish the influence zone and no influence zone in the simple and robust manners based on the RPFEM results. Its validity was verified by comparing it with the past data in the literature. The proposed equations provide great tools to evaluate and predict dangerous areas for shallow foundations in the vicinity of an identified underground cavity.

Chapter 4. Bearing capacity of a shallow foundation above the unsaturated soil with a cavity based on Rigid Plastic Finite Element

4.1 Introduction

In geotechnical engineering, the interaction between underground cavities and shallow foundations in unsaturated soil conditions presents a challenge that demands careful consideration. The stability and performance of foundations in such environments are profoundly influenced by the presence of voids beneath the ground surface. Underground cavities, including both natural voids and man-made structures, introduce complexities that extend beyond traditional foundation design assumptions. This introduction delves into the intricate dynamics of this interaction, emphasizing the important role of matric suction, a measure of negative pore water pressure in unsaturated soils, and its influence on the shear strength. As researchers have explored these phenomena, studies by Fredlund and Rahardjo (1993) and Vanapalli et al., (1996) have contributed valuable insights into the correlation between matric suction and shear strength in unsaturated soils, forming the basis for a comprehensive understanding of the challenges posed by underground cavities in foundation engineering.

Matric suction, a critical parameter in unsaturated soil mechanics, captures the tension within the soil water that arises due to soil moisture content being less than its saturated state. The relationship between matric suction and shear strength has been extensively studied to elucidate the mechanisms governing the behavior of unsaturated soils. Fredlund and Rahardjo (1993) emphasized the importance of matric suction in modifying the effective stress and, consequently, the shear strength of unsaturated soils. Their research highlighted that as matric suction increases, the effective stress in the soil also rises, resulting in enhanced shear strength. This finding has profound implications for foundation design, particularly in regions characterized by unsaturated conditions.

Moreover, Vanapalli et al., (1996) extended this exploration by examining the influence of matric suction on the shear strength of compacted unsaturated soils. Their work emphasized the role of suction-induced changes in soil structure and particle arrangement, further contributing to the understanding of how unsaturated conditions affect the mechanical properties of soil. By considering these seminal studies, it becomes evident that matric suction serves as a crucial parameter when assessing the stability of foundations, especially when situated above underground cavities. The interaction between underground cavities and shallow foundations is expected to become particularly pronounced when the design takes in account this matric suction. Shallow foundations typically spread their loads over a relatively large area and are more sensitive to variations in soil properties, making them susceptible to the presence of voids. The challenge lies not only in accurately assessing the load-bearing capacity of the soil but also in understanding how matric suction influences the shear strength and, consequently, the foundation's performance.

In regions with a history of karst formations or where man-made structures, such as tunnels or old mine workings, etc. create voids, the impact on shallow foundations is considerable. Karst terrains, characterized by soluble bedrock such as limestone, can develop extensive underground voids through dissolution processes. The unpredictability of these voids poses a significant challenge for foundation engineers, as the presence of such cavities can compromise the stability of shallow foundations. The system footing-cavity including hydraulic conditions, where are involved matric suction, and shear strength in unsaturated soils may significantly influence the stability and performance of shallow foundations. Drawing on foundational studies by Fredlund and Rahardjo (1993) and Vanapalli et al. (1996), this study introduces the results of the Bearing capacity of shallow foundation above the unsaturated soil with cavities. As the field of geotechnical engineering continues to advance, an understanding of these interactions is indispensable for developing robust foundation design methodologies that ensure the safety and longevity of structures in regions characterized by unsaturated conditions and the presence of underground voids.

Most up-to-date investigations address the issues of the ultimate bearing capacity of shallow foundations in unsaturated soils for soils without cavities (Garakani et al., 2020; Ghasemzadeh and Akbari, 2019; Tang et al., 2022; Vo and Russell, 2016). Fredlund and Rahardjo (1993) extended the equation of the ultimate bearing capacity equation of strip foundations for saturated soil mechanics to the unsaturated soils where the cohesion of unsaturated soils consists of two components, respectively the effective cohesion and a component due to the matric suction. They proposed the bearing capacity equations based on a stress state variable approach and a total stress approach. Oh and Vanapalli (2013) modified the total stress approach and the effective stress approach for the saturated soils to the unsaturated soils considering the influence of matric suction. Vanapalli and Mohamed, (2013) investigated the influence of parameters: matric suction, overburden stress, and dilation on the bearing capacity and settlement behavior of surface and embedded model footings in unsaturated sands. Vahedifard and Robinson (2016) derived the formulations of the shear strength theory of unsaturated soils along with complex numerical integration of average matric suction and simply linear variation of the suction stress, respectively. Their finding revealed that the bearing capacity of unsaturated soils is consistent with the shear strength behavior of unsaturated sands.

Investigations addressing the footing-cavity issue under unsaturated conditions are scarce. The shallow foundation can be in unsaturated conditions during its whole lifespan; thus, it is necessary to evaluate its performance under unsaturated conditions above the ground with cavities. The purpose of this study is first to investigate the performance of a shallow foundation above the ground with a cavity under the unsaturated state. Secondly, the study aims to clarify and establish the influence zone of the cavity on the footing under the conditions stated above by considering the shape and the location of the cavity, with an emphasis on the shear strength of the soils considered. The failure mechanisms are thoroughly examined to apprehend the influence of the generated matric suction on the footing-void system stability. Finally, a formula that accounts for the shear resistance parameters, as well as the geometry of the cavity, is proposed to predict the stability level.

4.2 Problem definition and boundary conditions

Figure 4.1 shows the footing-cavity system with a circular-shaped cavity. The seepage analysis and boundary conditions used consider the wall of the cavity as the drainage boundary. Assuming the ground is initially fully saturated, and the hydrostatic pressure is initially applied on the lateral boundaries, the seepage flow analysis runs until a steady state is established. It is noteworthy to mention that the hydrostatic pressure is applied to consider the pressure buildup beneath the footing induced by the presence of water. In addition, the hydrostatic pressure gradients drive the water within the soil, thus crucial for groundwater flow. During the seepage flow, additional incoming water such as rainfall is not considered. Briefly, it is a step-by-step simulation until the appearance of the unsaturated state layers within the soil. Similar conditions were used with the square-shaped cavity. The seepage analysis provides the porewater pressure distribution and the effective saturation degrees which are used in the mechanical equations of the RPFEM described later in this chapter following Yagi et al., (2010).

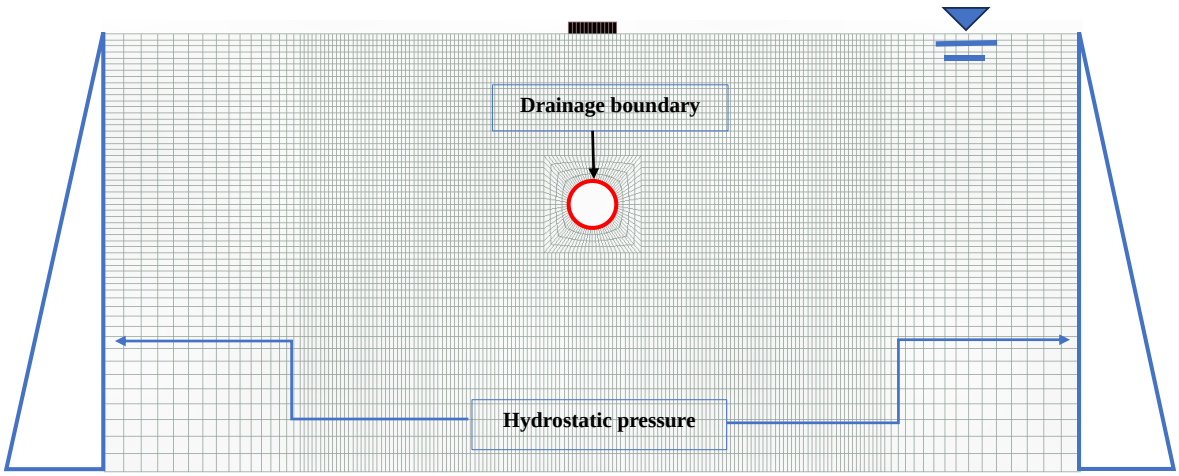

Figure 4.1. Footing-cavity system and seepage analysis boundary conditions

4.2.1 Analyses parameters

The analysis parameters described in Figure 3.1 were varied to evaluate the performance of the footing in unsaturated conditions. Table 3.1 shows the different ranges of values on geometry used in the analysis. Table 3.2 shows the soil properties used in the analysis. The properties considered for the footing are cohesion c = 50000 kPa and a shear resistance angle ϕ = 0 deg. to model a rigid footing. The soil-footing contact is assumed rough. Table 4.1 shows the parameters used for the seepage analysis based on the study by Sakai and Toride (2009).

Table 4.1 Seepage analysis parameters after Sakai and Toride (2009)

Parameters	Soil types	
	Cohesive (Silty Clay)	Intermediate (Silt)
Residual volume moisture content θ_r	0.07	0.034
Saturated volume water content θ_s	0.36	0.46
Permeability coefficient k (cm/day)	0.48	6
Van Genuchten parameter n	1.09	1.37

Details of bearing capacity analysis with the RPFEM in dry conditions have been provided in the previous chapter. This section introduces a few concepts of the considerations of unsaturated conditions with the RPFEM. Several attempts to define effective stress for unsaturated states have been undertaken (Bishop, 1960; Skempton, 1961). Most importantly, Fredlund et al. (1978) suggested that the strength of unsaturated soil is given by Eq. (4.1) where τ_f is the shear stress on the fracture surface and σ is the total stress, c' is the cohesion in the saturated state, ϕ_{net} is the internal friction angle based on the base stress and ϕ^b is a parameter that expresses the shear strength with increasing suction. The 3 terms on the right side indicate the increase in adhesion force due to the increase in suction.

$$\tau_f = c' + (\sigma - u_a)\tan\phi_{net} + (u_a - u_w)\tan\phi^b \quad (4.1)$$

Karube et al. (1996) proposed equations to account for the effect of suction as an increment of adhesive force. They expressed the cohesion as proportional to the suction and the effective saturation degree as:

$$c' = Se(\theta) \times s \times \tan\phi' \quad (4.2)$$

Where $Se(\theta) = \frac{\theta - \theta_r}{\theta_s - \theta_r}$ and $Se(\theta)$ is the effective saturation, ϕ' is the internal friction angle in the saturated state, s is the matric suction, θ_s is the saturated volume moisture content and, θ_r is the residual volume moisture content.

In this study, the seepage analysis considering the van Genuchten model (van Genuchten, 1980) provides the porewater pressure head distribution and the effective saturation degrees at a steady state. Subsequently, these data are used in the mechanical equations of the RPFEM with the consideration of Eq. (4.2) as shown in Yagi et al. (2010). This allows the effective stress analysis below the groundwater level, and the total stress analysis to take into account the effect of the apparent adhesive force due to suction to be considered above the groundwater level.

4.3 Methodology

In this section, parametric studies are performed to investigate the effects of the suction on the performance of the BC/BC_{NV} within *X* and *Y*. The works of Fredlund (2006); Fredlund and Rahardjo (1993); Oh and Vanapalli (2012); and Ravichandran et al. (2017) etc. inform us well regarding the contribution of the matric suction of unsaturated soils on the shear resistance of the soils, or well on the ultimate bearing capacity. Nonetheless, this raises the question of the applicability of this statement in the presence of the footing-cavity system. How is the stability increased or decreased under such circumstances? In addition, how is the deformation mode affected? The literature discussing the problem under such conditions is quite scarce, thus this section dedicates the investigation to this matter.

To obtain the distribution of the suction *s*, a prior seepage analysis is conducted with the RPFEM code, then follows the stability analysis which includes the results of the seepage analysis, and the porewater pressure distribution as shown in section 4.3. Table 4.1 summarizes the parameters utilized in the seepage flow analysis. At the initial conditions, the soil is assumed fully saturated and the ground water table is at the same level as the soil surface (Figure 4.1). Then, the water flows within the soil to the considered permeable boundaries until a steady state. These hydraulic drawdown conditions are similar to cases of inflow of water in unlined tunnel faces where the recharge rate is low and water inflow doesn't enter the system to replace the water lost in the tunnel (Shin et al., 2002). For the simulation in this study, it is important to note that during the seepage, there is no inflow such as rainfall or other sources of additional water input considered. Based on this series of analyses, the porewater pressure head distribution and the effective saturation degree S_e for several cases of the footing-cavity system are calculated. Although this distribution is influenced by the distance to the side boundary, the configuration used in this study is a more severe condition for the cavity with the unsupported walls under a high saturation degree condition that reduces the effective stress. Therefore, its bearing capacity and the influence zone by the cavity can be regarded as the safety side evaluation in this study.

4.4 Results

4.4.1 Seepage analysis

This section introduces the typical results of seepage flow presented in terms of the porewater pressure head distributions. Figure 4.2 shows the porewater pressure head distribution with the new water table (red dotted lines) within the ground with a square or a circular cavity at different locations. In this case, the parameters for the silty clay shown in Table 4.1 are used. The water table surface shape changes and has a funnel-like shape around the cavity. At larger distances *r*, where the cavity is close to the model's lateral boundary (Figure. 4.2 *g*-*h*), a serious asymmetrical condition of the depression cone is observed, but its influence on the bearing capacity is expected to be negligible because the footing exists on the opposite side. The unsaturated zone expands between the bottom of the cavity and the ground surface

according to the cavity location. Additionally, a large unsaturated zone is established right above the roof of the cavity compared to the one beneath the footing itself. For shallow cavities, the water table around the cavity at the steady state exhibits a small depression. In the deepest cavity cases, the water table drops down steeply around the cavities. In addition, it is suspected that the susceptibility to cavity instabilities increases because of the high saturation degree in the vicinity of the walls of the cavity combined with the increased soil self-weight. These distributions approximately align with the boundary conditions assumed as well as the study by Wei and Hudson (1990). Most importantly, the level of suction obtained depends on the SWCC parameters of the VG model assumed in Table 4.1, that is the increase of the suction s in the case of the cohesive and intermediate soils will differ respectively. In addition, there is a non-uniform strength distribution created within the soil layers such as the shallow depths have strengthened soil layers due to the negative porewater pressure (matric suction); and in deep depths, the soil layers are weakened because of the decrease of the effective stress with the saturated zone. Finally, the low initial water table position also influences the distribution of the suction in the unsaturated soil, but it is not considered further in this study because it leads more stable state.

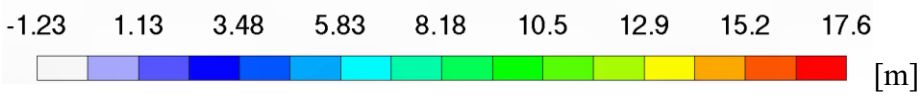

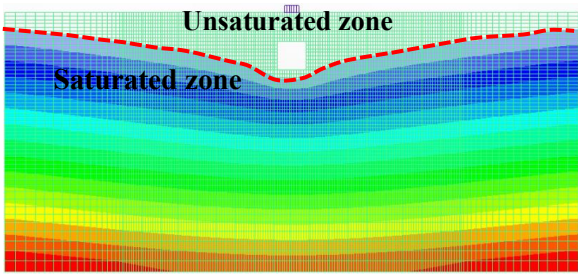

(a) Square cavity

B = 1 m, D = 2 m, h-$D/2$ = 2 m, r = 0 m

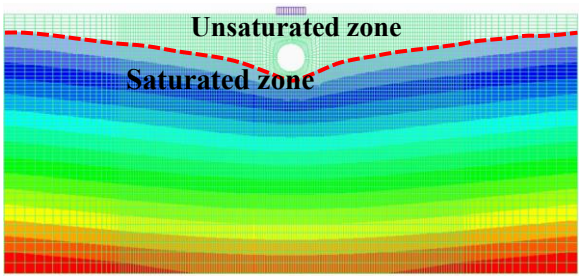

(b) Circular cavity

B = 2 m, D = 2 m, h-$D/2$ = 2 m, r = 0 m

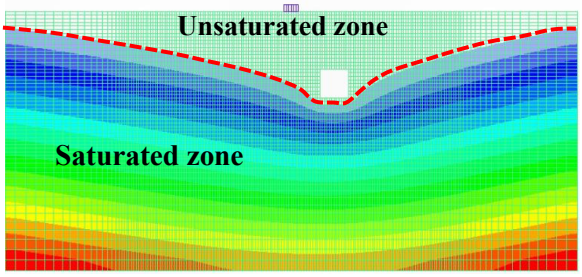

(c) Square cavity

B = 1 m, D = 2 m, h-$D/2$ = 4 m, r = 3 m

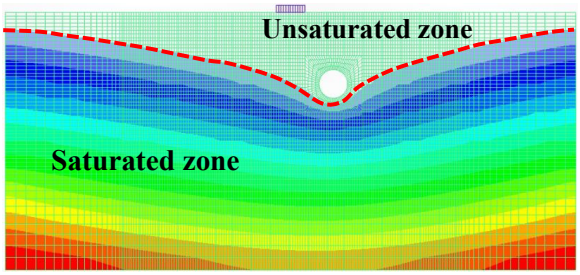

(d) Circular cavity

B = 2 m, D = 2 m, h-$D/2$ = 4 m, r = 3 m

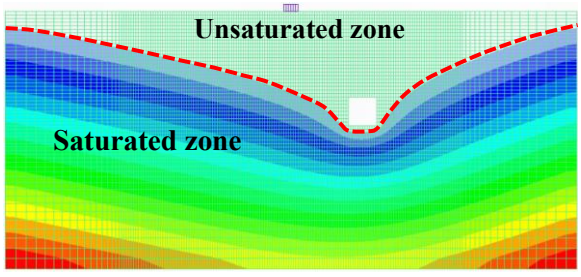

(e) Square cavity

B = 1 m, D = 2 m, h-$D/2$= 6 m, r = 5 m

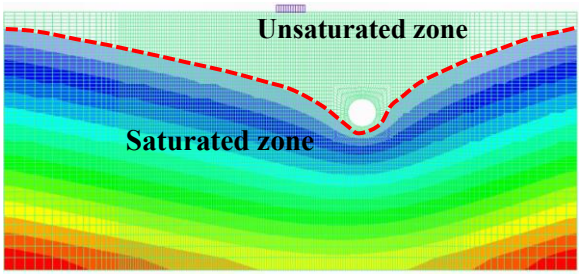

(f) Circular cavity

B = 2 m, D = 2 m, h-$D/2$ = 6 m, r = 5 m

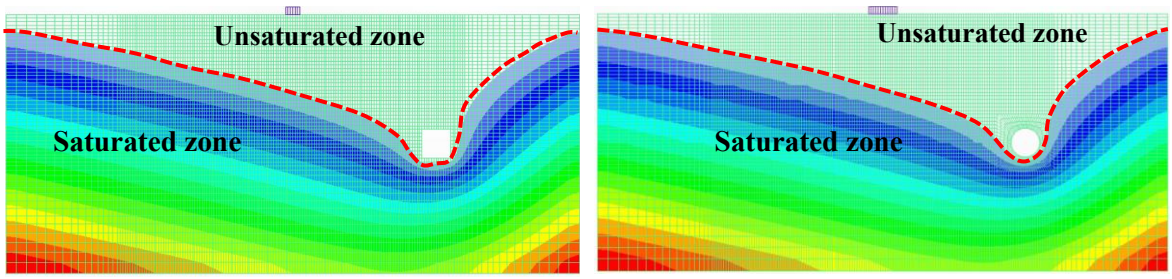

(g) Square cavity
B = 1 m, D = 2 m, h-$D/2$ = 8 m, r = 10 m

(h) Circular cavity
B = 2 m, D = 2 m, h-$D/2$ = 8 m, r = 10 m

Figure 4.2. Porewater pressure head distribution in the ground with the square and the circular cavities with variables h and r

4.4.2 Influence of the Cohesive Soil Materials

Figure 4.3 shows the variation range of the ratio BC/BC_{NV} (0.60 to 1.0) within the directions X and Y with a high cohesive material (c'= 50 kPa). X and Y axes are defined as previously in Chapter 3. The range of variation BC/BC_{NV} within the influence zone is higher than the allowable BC value. However, the influence zone is larger when compared with the dry conditions as shown in Fig. 3.7. The influence zone expands much in the vertical direction Y (up to Y = 3.75) and expands slightly in the horizontal direction (up to X = 1.70). The cause of this behavior is the high saturation degree in the vicinity of the cavity, resulting in void failure.

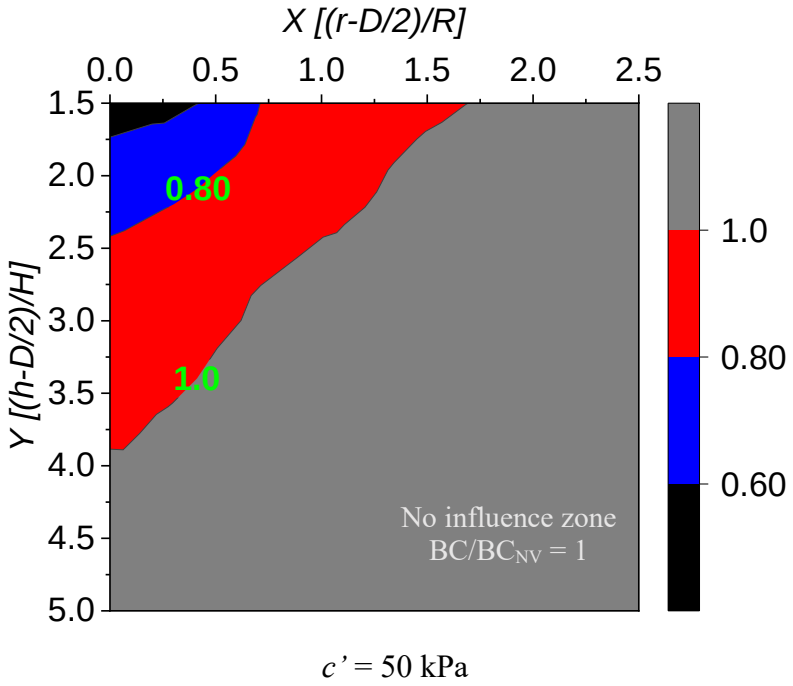

Figure 4.3. Distribution of BC/BC_{NV} within the *X* and *Y* directions for the unsaturated cohesive soil

4.4.3 Influence of the intermediate soil materials

Figure 4.4 shows the distribution of the BC/BC_{NV} within the *c*-ϕ soil with respectively *c*' = 10 kPa and ϕ'= 20 deg. and *c*' = 50 kPa and ϕ'= 30 deg. In Figure 4.4a, the distribution of the ratio BC/BC_{NV} elucidates the large expansion and influence in the vertical direction and a small influence in the horizontal direction. Noticeably, the black area which means $BC/BC_{NV} \leq 0.3$ appeared. It indicates the dangerous area where sudden and critical collapse of the ground is expected to happen. Figure 4.4b shows the distribution of the ratio BC/BC_{NV} when the cohesion and shear resistance angle are large. It is revealed that the influence of the cavity in vertical directions is decreased due to the high shear strength. The critical line in the horizontal direction is expected to be reduced for high values of ϕ', but the impact is less compared to the vertical direction. In addition, the area with $BC/BC_{NV} \leq 0.3$ does not appear in this case.

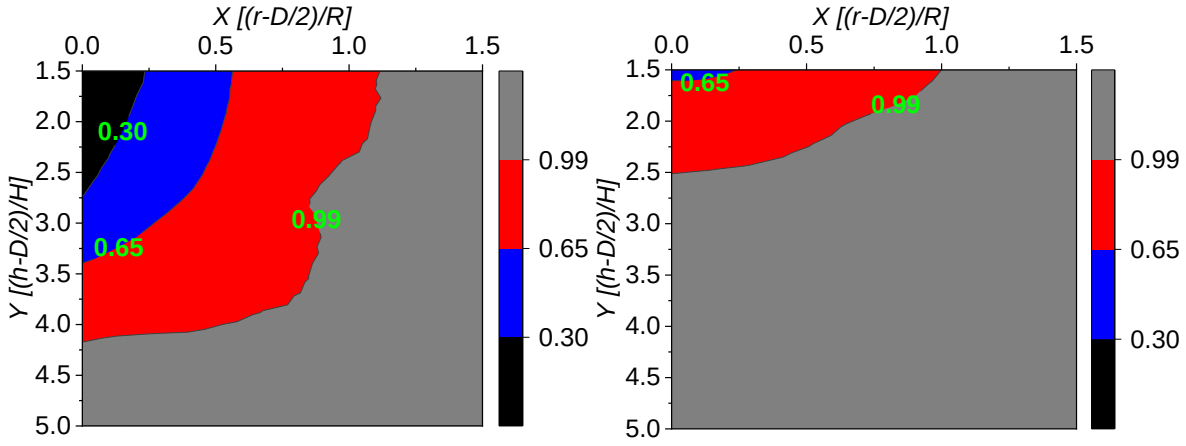

(a) c' = 10 kPa, ϕ' = 20 deg. (b) c' = 50 kPa, ϕ' = 30 deg.

Figure 4.4. Distribution of BC/BC_{NV} within the X and Y directions for the unsaturated intermediate soils

Overall, the similar tendency as the dry conditions is observed for the impact of the shear strength parameters on the influence zone, but the influence zone becomes wider in the unsaturated conditions than the dry conditions. The possible reason is explained by the difference in the failure pattern shown in the next section.

4.5 Comparative failure modes in dry and unsaturated conditions

This section displays some failure modes observed within the dry and unsaturated conditions at some selected locations of the cavity (r = 1 m, 5 m, and 10 m) considering the same geometrical settings and loading conditions. Here, the change of failure modes is shown for the square cavity for an intermediate soil material (c' = 10 kPa, ϕ' = 30 deg.) as the typical cases.

Figure 4.5a, b displays the failure modes for the cavity located at the depth (h-D/2) = 8 m and the horizontal distance r = 1 m. The dry condition case in Figure 4.5a (Bearing and Void failure) shows that the strain rate is also concentrated at the cavity wall (lower parts), but the main failure is recognized as the bearing failure. On the contrary, in the unsaturated condition, the change of the failure mode is striking because the failure occurs mainly at the cavity walls because of the reduction of shear strength due to the high saturation degree

around the cavities (Figure 4.5b, Void failure). The suction profile is high close to the soil surface; therefore, the strain rate is less beneath the footing and the failure surface extends from the footing edges to the cavity's walls suggesting a combined bearing and void failure occurrence at the footing level. Figure. 4.5c-f shows the differences in failure modes from the dry conditions to unsaturated conditions for the case that the cavity is horizontally far existing. It has observed that for deep cavities in the unsaturated soils conditions, the void failure is predominant. This is attributed to the decrease of stability due to less effective stress in the deep layers whilst the shallow layers deform less as they are strengthened with the matric suction effects. The farther the cavity exists horizontally, the less the interaction between the bearing failure and the void failure. However, a stronger interaction in the unsaturated conditions is observed than in the dry conditions. For shallow cavities in unsaturated conditions, it was also found an opposite trend to the situation with deep cavities. The predominant failure mode is the bearing and void failure although the increase of the shear strength due to matric suction. In addition, the interaction footing-cavity appears to reach larger horizontal distances.

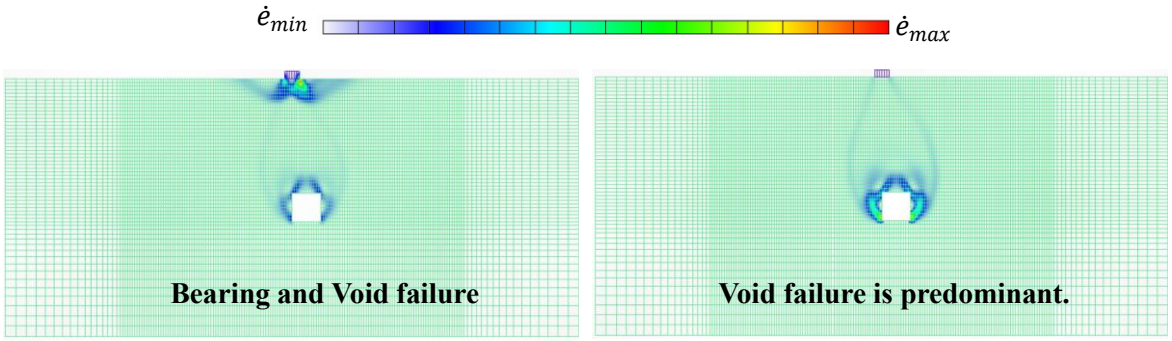

(a) Dry – Square cavity B = 1 m, D = 2 m, r = 1 m, h-D/2 = 8 m

(b) Unsaturated – Square cavity B = 1 m, D = 2 m, r = 1 m, h-D/2 = 8 m

(c) Dry – Square cavity B = 1 m, D = 2 m, r = 5 m, h-D/2 = 6 m

(d) Unsaturated – Square cavity B = 1 m, D = 2 m, r = 5 m, h-D/2 = 6 m

(e) Dry condition – Square cavity B = 1 m, D = 2 m, r = 10 m, h-D/2 = 2 m

(f) Unsaturated – Square cavity B = 1 m, D = 2 m, r = 10 m, h-D/2 = 2 m

Figure 4.5. Failure modes in dry and unsaturated conditions with the square cavity at the distance r

4.6 Influence zone and critical states equations

The distribution of the ratio BC/BC_{NV} within the space (X, Y) produced the critical lines shown in Figure 4.6 and Figure 4.7**.** From these figures, the critical lines are approximated as previously expressed as:

$$Y = pX^2 + q \tag{4.4}$$

Where $X = (r - \frac{D}{2})/R$ and $Y = (h - \frac{D}{2})/H$**.** The coefficients p and q are varied depending on the shear strength parameters and the conditions of the soils.

4.6.1 Influence zone in the unsaturated cohesive soils

The coefficients p and q for unsaturated cohesive soils are shown in Table 4.4. Figures. 4.6 shows the critical lines for unsaturated cohesive soils based on the RPFEM results and the proposed equation Eq. (4.4) using the coefficient shown in Table 5a.

Table 4.4. Coefficients p and q are based on the RPFEM results. Cohesive soils

Coefficients	Unsaturated condition
p	-5.03
q	3.87

A good agreement is observed between the RPFEM results and the proposed equation. It can be expressed from the comparison of these coefficients that the influence zone is deeply expanded and sharply changed in the horizontal direction in the unsaturated condition.

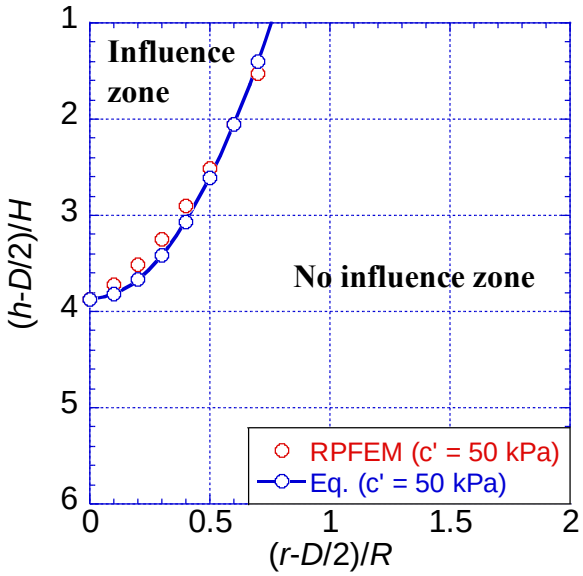

Figure. 4.6 Critical line in unsaturated cohesive soil (c' = 50 kPa)

4.6.1 Influence zone in the unsaturated intermediate soils

The coefficients p and q for the dry and unsaturated intermediate soils are shown in **Table 4.5**. **Figure 4.7** shows the critical lines for unsaturated intermediate soils based on the RPFEM results and the proposed equation Eq. 4.4 using the coefficient shown in **Table 4.5**. It shows a good enough agreement and evaluates the critical lines on the safe side although a small discrepancy is observed. It can be expressed from these coefficients that the influence zone is influenced more by both the cohesions and the shear resistance angle. Additional parameters such as the unit weight of the soils and the footing size are included into the equations to account for their influence.

Table 4.5. Coefficients p and q as function of the soils'strength parameters. Intermediate soils

Coefficients	Unsaturated condition
p	$a_0 \tan\phi' \left(\frac{a_1}{a_0} + \frac{a_2}{a_0}\tan\phi' + \cot\phi'\right)$
q	$b_0 \tan\phi' \left(\frac{b_1}{b_0} + \frac{b_2}{b_0}\tan\phi' + \cot\phi'\right)$
a_0	$-13.02 + 3.89 \times \left(\frac{c'}{\gamma B}\right)$
a_1	$41.76 - 24.34 \times \left(\frac{c'}{\gamma B}\right)$
a_2	$-33.53 + 23.66 \times \left(\frac{c'}{\gamma B}\right)$
b_0	$13.45 - 2.71 \times \left(\frac{c'}{\gamma B}\right)$
b_1	$-26.612 + 6.06 \times \left(\frac{c'}{\gamma B}\right)$
b_2	$16.40 - 3.56 \times \left(\frac{c'}{\gamma B}\right)$

Based on the above discussion, the proposed solutions can help determine the influence zone of the cavity on the UBC of the footing resting on various types of soils, while depending on the soils strengths parameters. In addition, it is possible to determine the necessary depth and radius to investigate the presence of the cavity in practical engineering and also helps to predict the failure mechanism of the footing-cavity system.

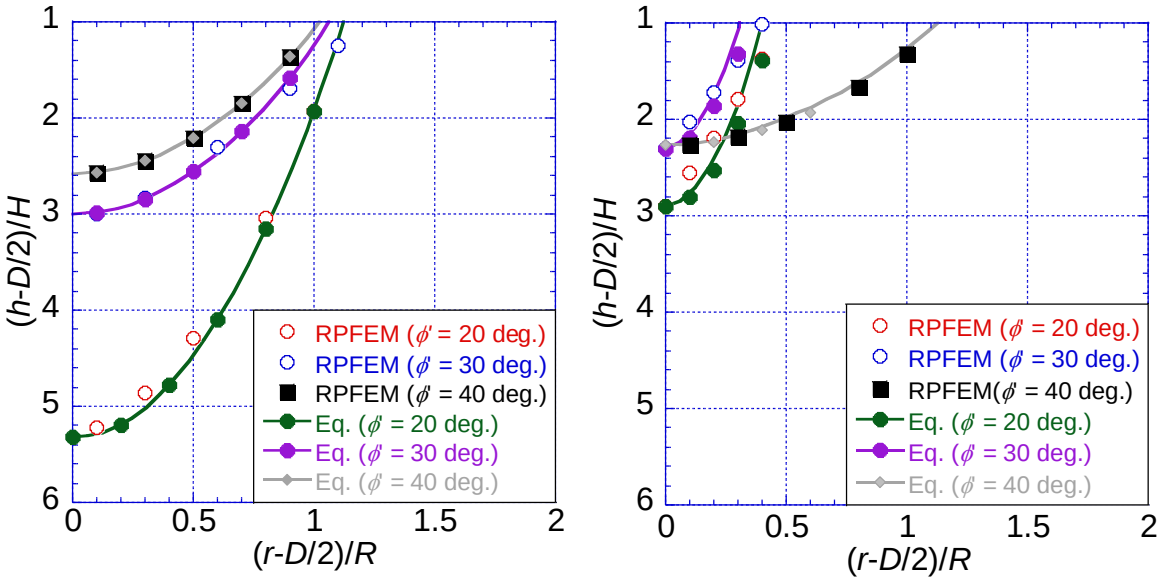

(a) Small cohesion (c' = 10 kPa) (b) Large cohesion (c' = 50 kPa)

Fig. 4.7 Critical lines in unsaturated intermediate soils with variable ϕ'

4.7. Conclusion

The seepage analysis provided a comprehensive distribution of the porewater pressure within the soil materials. It revealed the non-uniformity of shear strength due to negative porewater pressure above the water table and reduced effective stress near the water table and the vicinity of the cavity. This distribution played an important role in the distribution of the bearing capacity ratio BC/BC_{NV} as well as the failure modes. The analysis of the BC/BC_{NV} within the normalized plan (X, Y) illustrates the different ways of the expansion of the influence zone of the cavity towards the footing. In addition, the comparison to dry conditions showed that the expansion in unsaturated condition was much larger than the one observed in dry conditions considering the same geometries and effective strength parameters. The influence zone extension is wider compared to the dry conditions as the saturation around the cavity is higher and induces instability. The failure modes were also analyzed and compared with the dry conditions results. A drastic change in which the void failure was predominant for deep cavities. However, at the shallow depth where large frictional angles were considered, the bearing and void failure were predominant. The soils with low frictional,

angle values showed a predominance of the general bearing failure. The equations of influence zone are proposed to distinguish the influence zone and no influence zone in simple and robust manners based on the RPFEM results. A tentative of the validation of these analyses is conducted to confirm these assumptions with the experimental testing in the next chapter. The proposed equations provide great tools to evaluate and predict dangerous areas for shallow foundations in the vicinity of an identified underground cavity in unsaturated conditions.

Chapter 5. Experimental analysis of the UBC on the sandy soil with a cavity in dry and unsaturated soils.

5.1 Introduction

The development of underground cavities has been shown to lead to severe ground collapse in urban areas. This occurrence induces, either from the initial stage or during their expansion stage, ground displacements ranging from a few millimeters to several tenths of meters. (Augarde et al., 2003; Guo et al., 2013; Mukunoki et al., 2012). Before the collapse, the cavity induces shear strength losses within the soil, consequently on the performance of the nearby engineering structures, foundations, piers, etc. Several researches have been carried out based on the conventional saturated soil mechanics. These considerations might lead to underestimation of the bearing capacity in the design processes, especially for semi-arid areas or areas prone to collapse with important fluctuations of the underground water table, where the foundation can be under unsaturated condition for its entire lifespan.

Most of the studies investigating this issue focus on the analysis of internal erosion with a focus on dams (Foster et al., 2000), or pipes which involve the soil discharging into cracks of sewer pipes leaving a cavity above. In these categories, due to differences in the process of cavities appearances, two main classifications exist concentrated leak erosion in core zones and internal instability in filter zones. Concentrated leak erosion is the enlargement of cracks in the core of high-pressurized water, while internal stability is a migration of the finer fraction through the coarser fraction with the seepage flow (Sato et al., 2015). To our knowledge, there have been no recent studies on the analysis of the Bearing capacity of footing on soils with cavities under unsaturated conditions or considering different hydraulic conditions and the effect of the matric suction on the overall stability and performance of the footing. Sinkholes have been reported to appear near structures in urban areas and statistically occur in rainy seasons, which is dangerous as the ground is in saturated conditions. This leaves unanswered questions regarding the behavior of the involved

structures in unsaturated conditions (Dry seasons) where probable fluctuations in the water table can be considerable and little is known about this phenomenon (Nygren et al., 2020).

This chapter introduces the experimental analyses conducted on unsaturated sandy soil with cavities. To achieve this objective, at first, a series of model tests on dry soil sands with different relative densities are conducted. Subsequently, with fully saturated conditions of soils without cavities, the UBC of the footing is analyzed. Then follow a series of unsaturated tests without and with cavities. Finally, in the last series of model tests, a simulation of the internal erosion involving an initial small cavity simulated through the metallic pipe, the UBC of the footing is conducted. A simple laboratory scale simulation method of the cavity as well as a cavity generation from the initial appearance of the cavity and their respective influence on the ultimate bearing capacity of the footing is developed. The series of model footing tests were conducted on unsaturated sandy soil with a cavity considering different vertical positions of the cavity as well as the water table. The cavity was created using an easily found commercial balloon, placed, and expanded within the model soil. The unsaturated soil was vertically loaded using a circular model footing of diameter B = 30 mm after the balloon was deflated. Based on experimental results, a simple analytical UBC was developed for sandy soil under unsaturated conditions.

5.2 Experimental setup and testing program

The experimental setup used to analyze the Ultimate Bearing Capacity of the footing on sandy soil with a cavity is shown in Figure 5.1. The experimental device is an acrylic tank built with a cylindrical shape to receive the soil model. The circular base has an inner diameter D_t = 300 mm. The tank has a built-in porous stone fixed at the bottom. On the base, the external part is mounted with several valves serving for upward injection of water as the well water draining out. The soil tank has 5 holes on its lateral surface on which are connected water pressure gauge can be attached. During the cavity creation process, the water pressure gauge is replaced by a set of pipe connectors. The drained-out water is collected through a set of plastic tubes. The tank is mounted on its top with a lid that receives the loading device. The loading device has a rod to which is attached the circular metal plate (footing) passing

through the central opening of the lid. To the loading device is associated the strain gauge for displacement measurements. A Handle helps with manual movements of the rod. However, a motor connected through an electric wired connection commands the downward and upward movement of the rod, thus the loading speed.

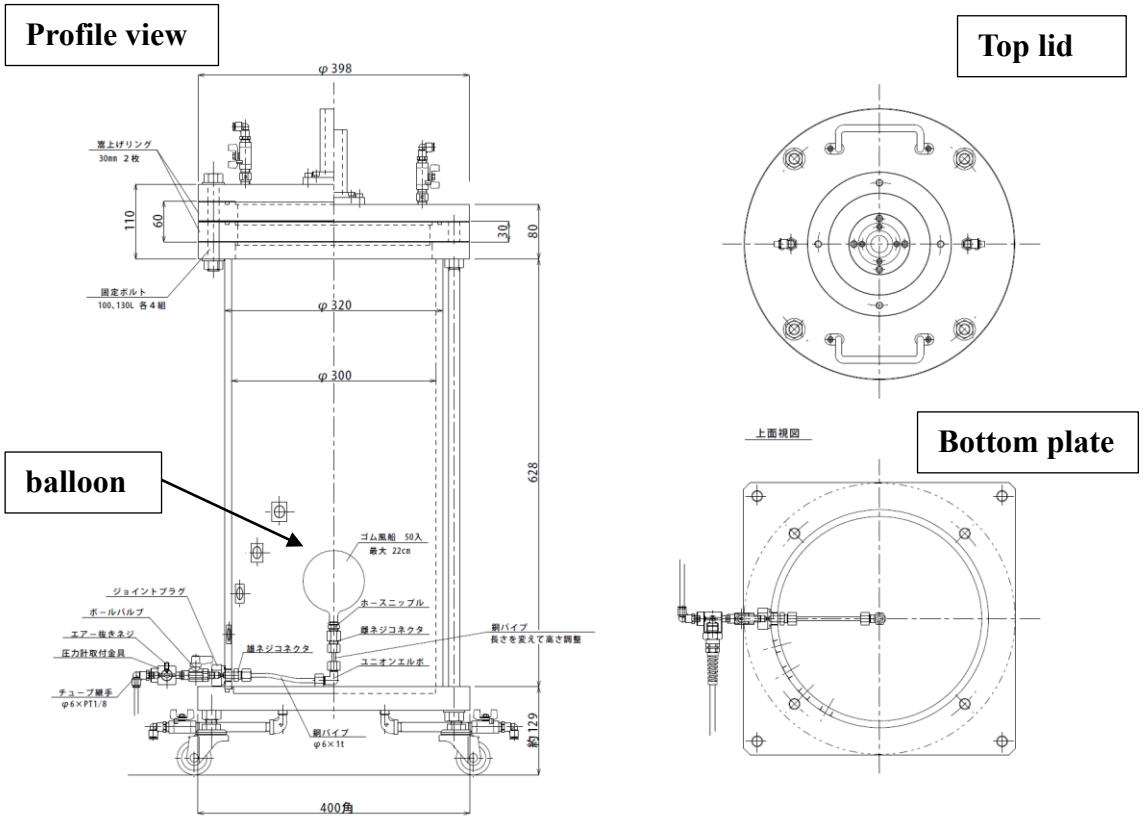

(a) Schematic view of the experimental apparatus- (profile view, top lid, and bottom porous stone)

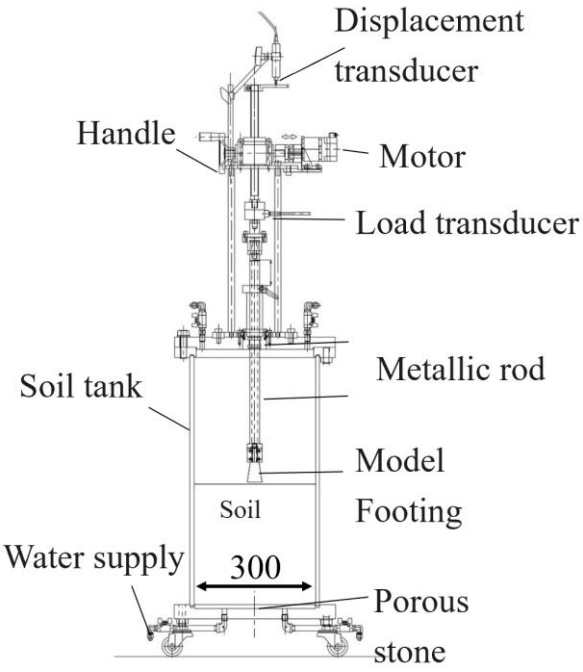

(b) Schematic view of the experimental apparatus with the soil model.

Figure. 5.1: Overview of the experimental apparatus for the experimental UBC analysis against sandy soil with cavity.

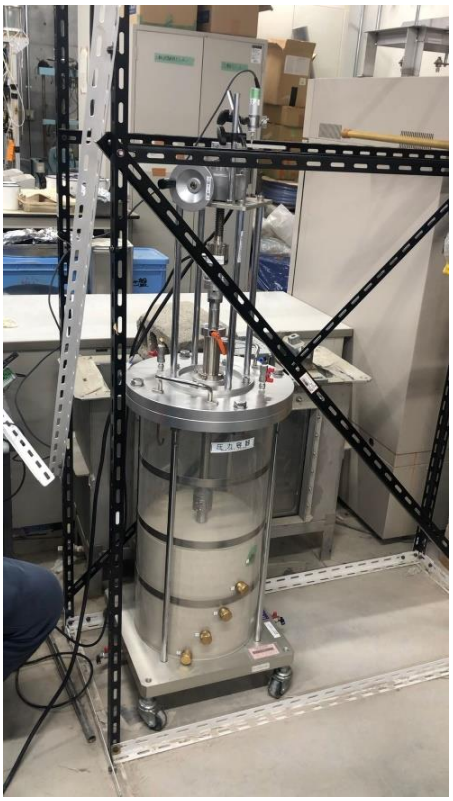

Figure. 5.2 Photos of the experimental apparatus with the soil model

The loading speed is set at 0.5 mm/min. The soil used is silica sand No. 7 and prepared in layers of 30 mm. The choice for this material is based on its availability and reusability. The soil properties are summarized in Table 5.1.

Table 5.1. Properties of the soil used.

Soil type	Dry unit weight γ_d (kN/m^3)	Relative density D_r (%)
Silica sand No. 7	14.8	70

For practical reasons, the soil with D_r = 70% was maintained for the most of analysis to avoid looseness and soil failure before loading tests. The soil model was prepared in 10 ten layers of 30 mm each. To ensure horizontality, leveling with a brush on the surface of each was conducted and horizontality was confirmed with a laser measurement. The observations of

ground failure were solely monitored after loading. However, the soil displacements and loading magnitude increments were monitored through the PC screen. Visual observations are also possible through the acrylic tank.

5.3 Testing program and conditions

Table 5.2 lists the details of the testing conditions. For the analysis cases without cavity, the soil with relative dry density D_r of 60% and 70% were used. The positions of the cavity are chosen to be the closest possible to the axial position of the footing/top lid of the apparatus.

Table 5.2. Tests conditions

Experiments conditions	Relative dry density *Dr* (%)	Depth of cavity (*h*-*D*/2)	Water level
Dry soil without cavity	60, 70	-	-
Saturated soil without cavity	60, 70	-	Above soil surface
Unsaturated soil without cavity	70	-	Variable
Dry soil with cavity	70	Variable	-
Unsaturated soil with cavity	70	Variable	-
Unsaturated soil with cavity	70	Fixed	Variable
Initial small cavity	70	Fixed	Fixed.

The process of cavity creation implemented in this work is cost effective and does not necessitate heavy equipment or centrifugal testing which is an advantage. Figure 5.3 illustrates the cavity creation with the ballon, soil models etc.

Figure 5.3. Soil with cavity preparation and Balloon insertion within soils layer at desired position.

As for the unsaturated conditions, Figure 5.4a illustrates the ideal conditions for its realization.

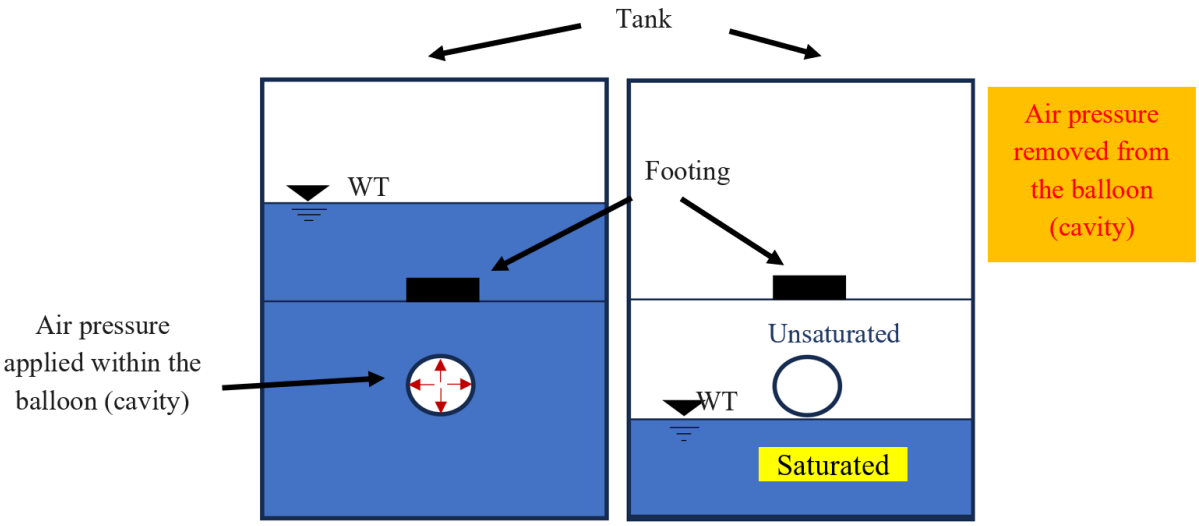

Figure 5.4a Illustration of creation of unsaturated soil condition with cavity.

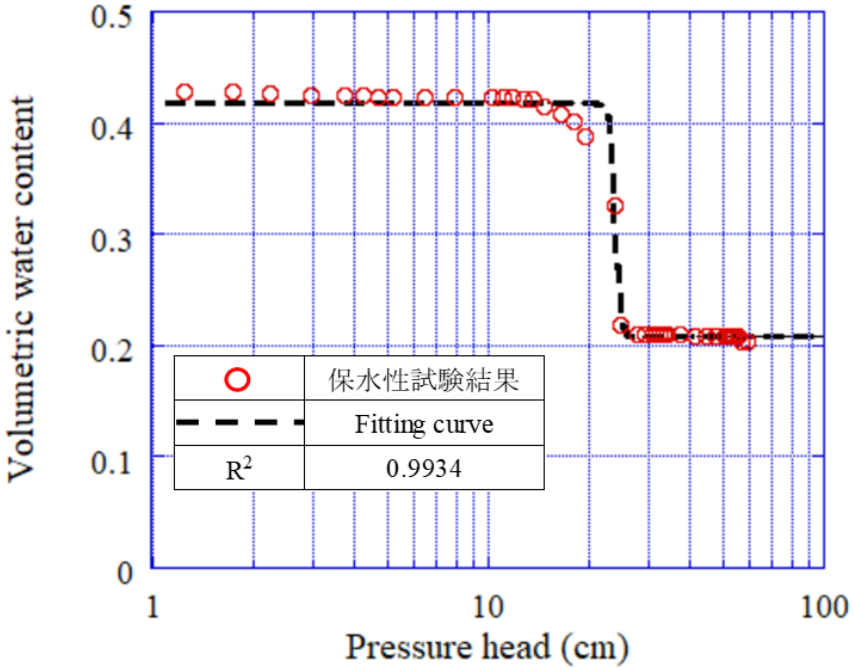

Figure 5.4b. SWCC curve obtained from test on silica sand No.7

The dry soil is first prepared in layers within the soil tank. The soil is initially saturated (fully) by upward injection of water through the valve connected to the bottom porous stone. To ensure full saturation, the water injected needs to cover the entire soil surface and occupy all the voids in the sand. The unsaturated phase is obtained by draining out the water through the application of the air pressure from the valve on top of the lid. The air pressure applied was 500 kPa. Care was taken to avoid the application of high values of air pressure that might lead to consolidation of the upper layer of the soil model. The drainage of water is adjusted to reach the water table as shown in Figure 5.4a. An interval time of 24 hours is allowed for the soil moisture to reach a steady state, ensuring then an unsaturated state to established between the water level and the soil surface. The results of the water retention test were fitted using van Genuchten's equation shown below:

$$s_e = \left[\frac{1}{1+(\alpha|h|)^n}\right]^m \text{ with } m = n - \frac{1}{n} \tag{5.1}$$

5. 4 Results and Discussions

5.4.1 Loading tests in dry conditions and saturated sand without cavity

Results of loading tests with a circular footing type are reported in Figure 5.5 as the load versus displacements under dry conditions and saturated conditions. The distinct relative density D_r used for calibration purposes and helped in choosing the adequate soil with enough strength for analyses in cases with the cavity as will be introduced in the next sections.

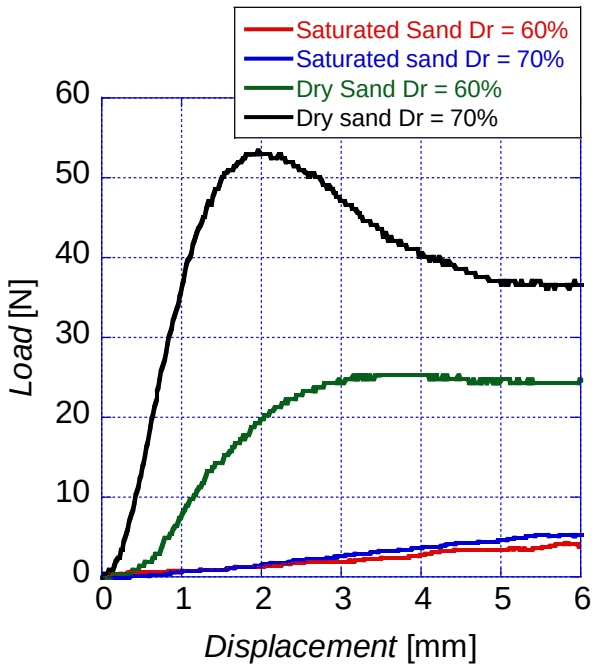

Figure. 5.5 Load vs displacement results of dry and saturated soils without cavity at relative density D_r = 60% and 70%.

Figure 5.5 illustrates that for the dry conditions with Dr = 60% (green curve), at initial stages up to approximately 2 mm, there is initial linear behavior revealing an elastic deformation phase. The deformations in this region are proportional to the applied load. Between 2 mm and 3 mm, a nonlinear phase is observed, revealing a transitional stage to the yielding or residual strength of the soil. From 3 mm displacement a plateau is observed showing that the displacements are minimum under load increment, which is quasi stable condition. The UBC is calculated at 3 mm displacement as recommended in the Japanese

construction code (displacement corresponding to 10% of the footing width). The soil with D_r = 70% (Black curve) showed a similar linear increase at the initial stage of loading up to 1.5 mm displacement. However, a clear peak in the curve was observed. This represents the maximum load this soil can withstand and the UBC was calculated at this point. The post-peak behavior for this soil (D_r = 70%) showed a smooth and linear decrease in the settlement level for each load increment before reaching a plateau. Comparatively, the residual strength is expected to be higher for the soil of D_r = 70% than for the soil of D_r = 60%. In addition, at their initial stages, it can be seen that the stiffness is expected to be higher for the soil of D_r = 70%.

The curves in red and blue color represent the results of loading tests on saturated soils at initial dry relative densities of 60% and 70% respectively. The curves in saturated conditions show linear behavior from the initial stages and continuously over 5 mm of settlement. The stiffness in both soils modeled is relatively similar. However, compared to the dry conditions, there is a decrease in the stiffness of the soil due to the presence of water. The excess porewater pressure build-up reduces the effective stress and greatly the overall soil strength. No peak load was observed for either of the considered soils. Thus, the UBC was estimated at the displacement corresponding to 10% of the footing width *B*, i.e. 3 mm. In light of the observations above, the soil of *Dr* = 70% was maintained for the rest of the analysis with cavities. **Table 5.3** below summarizes the results of the calculated ultimate bearing capacity.

Table 5.3 Values of Ultimate Bearing Capacity for soils without cavities in dry and saturated conditions.

Relative density *D*r (%)	Dry Silica Sand		Saturated Silica Sand	
	Peak load or at 10% of *B* [N]	UBC [kN/m^3]	Peak load or at 10% of *B* [N]	UBC [kN/m^3]
60	25	32.55	3.1	1.53
70	53.1	72.27	3.6	2.24

5.4.2 Loading tests in Unsaturated conditions without cavity

This section introduces the results of loading tests on soils without cavities under unsaturated conditions. The soils with the relative dry density of D_r = 70%, in initial dry conditions, were saturated through an upward water injection as described in the previous section. Figure 5.6 shows the curve of load test under unsaturated conditions. The observed behavior of the unsaturated soils shows a linear increase of the displacement with the load increment. No clear peak or yield point is observed, thus for the estimation of the bearing capacity, the displacement at 3 mm is retained for the estimation of the UBC. The matric suction value was not measured clearly. However, the result shows that the UBC is increased in the unsaturated condition. This confirms a buildup of the negative porewater pressure that enhances the soil strength.

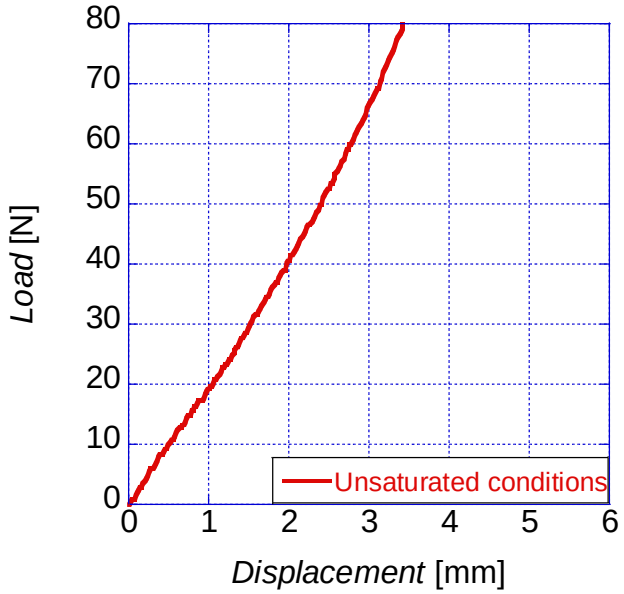

Figure. 5-6. Load – Load-displacement results unsaturated soils without cavity at relative density D_r = 70%.

Table 5.4 shows the values of UBC for the soils in dry and unsaturated conditions. It is noticeable that the increase in the value of the UBC in unsaturated conditions by 1.9 times as compared to the dry conditions. The results confirm the conclusions of claims of matric

suction influence of the shear strength of the soil (Garakani et al., 2020; Costa et al., 2003; Rojas et al., 2007; Vanapalli et al., 2013).

Table 5.4. Values of Ultimate Bearing Capacity for soils without cavities in dry and saturated conditions.

Relative density	Dry Silica Sand.		Unsaturated Silica Sand	
*D*r (%)	Peak load or at 10% of *B* [N]	UBC [kN/m^3]	Peak load or at 10% of *B* [N]	UBC [kN/m^3]
70	53.07	72.27	73.41	101.06

5.4.3 Bearing capacity tests with a balloon-type cavity in dry and unsaturated sandy soil

Figure 5.7 shows the results of loading tests on the soil models in dry conditions when the balloon is inserted to simulate the presence of the cavity. The balloons inserted in the soils were prepared for the diameter of cavity D = 60 mm.

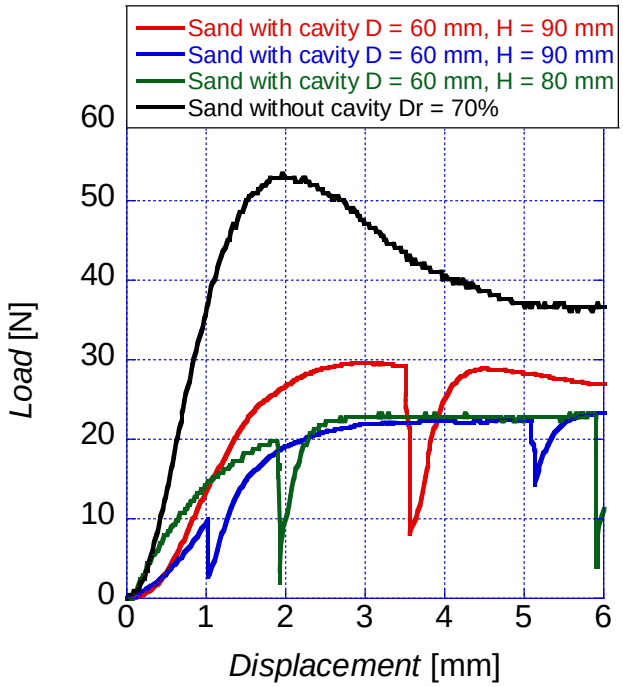

Figure. 5.7 Load vs displacement for dry soils with cavity

However, the sandy materials did not have enough strength to withhold the stress release due to air pressure removal from the balloon. Thus, the soil on the central part simultaneously settled at each air pressure release. Then, an approach of loading step by step after each air pressure release was implemented. The load was applied after 1 mm, 2mm, and 3 mm of displacements successively. The reported cases portray the cases when the cavity depth is H = 80 mm and 90 mm. It is revealed that the cavities close to the surface of the model soils yielded a high influence of the UBC of the footing by reducing sensibly its value as compared to the no cavity condition curve in the plot. This staged loading is necessary because it reveals the short-term behavior of such soil. The loading after 2 mm and 3 mm of displacements reveals also the residual state of soil's strength after collapse which is much lower compared to the residual strength in the no cavity condition.

Table 5.5. Values of Ultimate Bearing Capacity for soils with cavities in dry conditions.

Test cases (Depth of cavity (*h-D*/2), Diameter *D*)	Loading conditions and obtained UBC		
	Displacement before loading [mm]	Peak load or load at displacement = 10% of *B* [N]	UBC [kN/m^3]
h-D/2 = 90 mm, D = 60 mm	1	22	28.29
h-D/2 = 80 mm, D = 60 mm	2	22	28.29
h-D/2 = 90 mm, D = 60 mm	3	30	39.61

The experimental analysis was carried out on the unsaturated soils with cavities. Figure 5.8 displays the load vs displacement for cases experimental cases when the cavity location is at respectively 60 mm, 100 mm, and 110 mm. The diameter of the balloon is kept at the same dimension of *D* = 60 mm. The water table before loading is adjusted to fit the bottom of the cavity as in Figure 5.4. These configurations make possible the existence of different matric suction configurations. The load settlement curves illustrate that the cavity near the soil surface (*h-D*/2 = 60 mm) has more influence on the UBC as the collapse load is the lowest for all the cases. This is due to the high saturation degree and the less negative porewater pressure buildup within the soils. In addition, the load versus displacement curve

(blue) shows or reaches a plateau quickly before 3 mm displacement. With a cavity at *h*-*D*/2 = 100 mm, there is an improvement of the UBC. This is explained by the facts that the cavity is deep enough to withstand the soil self-weight. In addition, the unsaturated shear strength of the soil is increased by the level of matric suction generated. When the cavity is located at depth *h*-*D*/2= 110 mm, the load vs displacement shows a linear behavior. The load considered at 3 mm displacement is larger comparatively to the two other cases. The influence of confining stress, the unsaturated strength provides more strength to the soil. Table 5.6 summarizes the results of UBC obtained the different analysis.

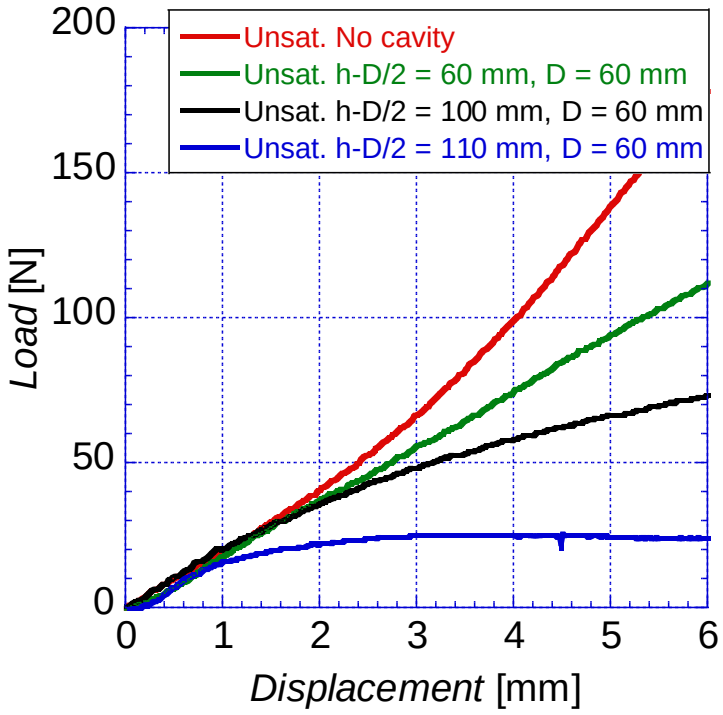

Figure 5.8. Load vs displacement for unsaturated soils with cavity

Table 5.6. Values of Ultimate Bearing Capacity for soils with cavities in unsaturated conditions

Test cases (Depth *h-D*/2, Diameter *D*)	Loading conditions and obtained UBC		
	Saturation degree Sr [%]	Load at displacement of 10% of *B* [N]	UBC [kN/m^2]
h-D/2 = 60 mm, D = 60 mm	47.9	24.8	31.23
h-D/2 = 100 mm, D = 60 mm	32.3	48.60	65.24
h-D/2 = 110 mm, D = 60 mm	29.8	56.05	76.49

A photo of the soil with a cavity created is shown in Figure 5.9 proving that the cavity was successfully created.

Figure 5.9. Post loading showing evidence of Cavity created.

In light of the results of the UBC, the conclusions drawn from the numerical analysis with the RPFEM are confirmed here. The cavity in deep layers of the soil has less influence on the performance of the footing.

5.4.4 Bearing capacity tests under Unsaturated soils with cavity and WT level changes

The current section introduces the results of the model tests simulating the cavity at initial stages. Cavities with small diameters are simulated with small diameters and variable height $h_{c.}$ The cavities created using this approach are similar to the study showing the appearance of the cavity as a crack or at initial stages. The UBC analysis is of importance in this approach as it provides degrees of reduction of the performance of the footing. The illustration of this testing setup is illustrated in Figure 5.10. The cavity is created using a column of sugar placed in advance in a pipe at the center of the soil tank. As the soil is inserted layer by layer, and then saturated. By the application of air pressure at 50 kPa, the water melting the sugar is drained out leaving a hollow in the center of the soil model. It is worth noting that the contact pipe and soil.

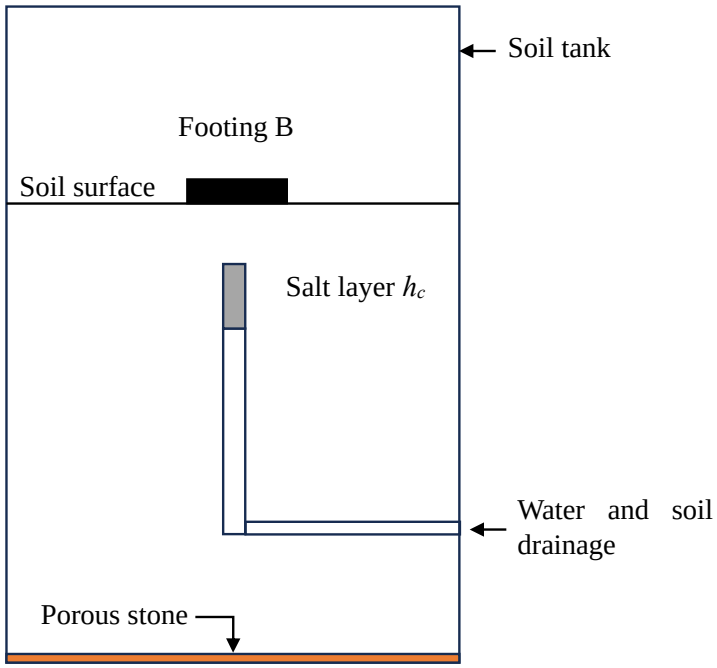

Figure 5.10. Illustration of model setup with initial cavity.

The results of these analysis cases are shown as load versus displacements as well. Figure 5.11 highlights the results of model tests conducted in this section. The cases L0, L15, L45, and C6 represent the cases where initial cavity heights h_c are respectively 0 mm, 15 mm,

30 mm, and 45 mm. Due to unsaturated conditions, the linear behavior between load and displacement is observed for the analyzed cases. The cases without initial cavities (Lo) show the highest stiffness, consequently producing the highest value of the UBC. The impact of the cavity at the initial stages is then observed through cases L15, L45, C6 which show a decrease in the collapse pressure (Load per unit area) taken at 3 mm of displacement.

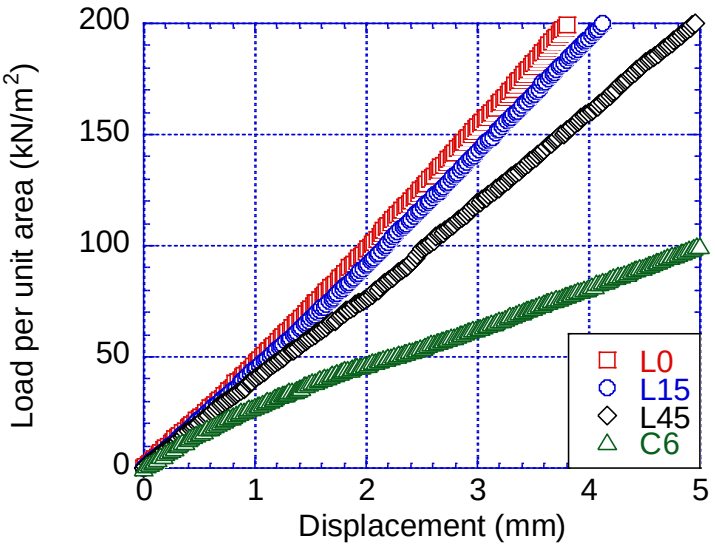

Figure. 5.11. Load vs displacement for unsaturated soils with small initial cavities

5.5 Discussion

Different model tests were introduced in this chapter and an emphasis on the unsaturated soil conditions was investigated. From, model tests in dry conditions, saturated conditions, and unsaturated conditions, the majority of cases showed a linear behavior load vs displacement. For the cases where this relationship did not show a peak, the ultimate load was considered at the displacement of 3 mm corresponding to 10% of the footing width *B*. The results of UBC in unsaturated conditions showed a great increase compared to the tests in dry conditions. Even though, the design of model tests lacks a device to measure precisely the negative water pressure build-up, the effect of the matric suction increasing the shear strength of the soil was observed through the values of the UBC for dry and unsaturated conditions. The water level and fluctuations within the soil portray that different levels of matric suction and the UBC vary accordingly. The results of model tests with cavities showed that the deeper

the cavities had less influence on the performance of the footing, confirming the results of numerical analysis with RPFEM. In dry conditions, even though it was difficult tests to model, an insight into the performance of the footing was observed. The dry sand did not hold enough to self-support the void walls created as the sand particles suddenly failed at the removal of air pressure. The results in unsaturated conditions have shown greater UBC compared to the cases in dry and saturated conditions. The results of the tests with the initial cavity revealed a decrease in bearing capacity at the initial stages. This study has the merit to embrace a neglected approach up to now regarding the behavior of the shallow foundation above the ground with a cavity. Although the matric suction increases the shear strength of the soil, we need to think about the 'apparent stability' provided by the unsaturated condition in the long term. The collapse of underground cavities is usually sudden, and the water table fluctuates during the life cycle of the foundation. This approach with the revealed trade-off relationship of matric suction and effective stress might be a key to solving the problem.

5.6 Conclusion

Several model tests, introducing an easy and cost-effective technique to simulate the cavity in the ground with easily found commercial balloons, were conducted on the ground with a cavity under unsaturated conditions. The trade-off relationship was observed between matric suction and effective stress; giving higher values of ultimate bearing capacity in deeper layers and lower ultimate bearing capacity at a shallow depth of the cavity, compared to the cases without consideration of the groundwater table. The RPFEM results in the cases with the cavity beneath the footing ($r/D = 0$) are confirmed with the reproduced model tests with ultimate bearing capacity observed in the model tests increasing with both the matric suction and the depth of the cavity. The results can help in understanding the sudden collapse of cavities in the long term as the water table fluctuates within the ground as well as the expansion of the influence zone of a cavity under the observed conditions. Although the measurement of matric suction and saturation degree was not done directly in the present experiments, the designed process proved to be reliable in modeling the ground with a cavity. In addition, the model tests showing the influence of initial cavity appearance on the bearing capacity showed reasonable results, providing an understanding of how stability evolves.

Chapter 6. General conclusions and Recommendations for future research work

6.1 General conclusion

This study investigated the bearing capacity of the footing situated on soil with cavities under dry and unsaturated conditions. The soil types considered are cohesive and intermediate soils. The study investigation was undertaken under two distinctive approaches:(1) A numerical analysis approach considering the abovementioned soil types under dry and unsaturated conditions. The numerical analyses were conducted using the Rigid Plastic Finite Element Method RPFEM. The RPFEM is used in plane condition with the Drucker Prager as yield function. (2) Experimental model tests were conducted on Silica sand No. 7 in the same conditions, with a cavity created using a commercial balloon. Based on Numerical analyses, the influence zone equations in dry and unsaturated are proposed. Detailed conclusions can be found in each preceding chapter. More general conclusions are summarized as follows:

- In Chapter 2, based on the comprehensive literature review on the studies of the Bearing Capacity of shallow foundations with cavities, the needs to provide a solution and equation of the influence zone were emphasized.

- In Chapter 3, based on the RPFEM, the bearing capacity of the footing laying on several soil types is conducted. The location of the cavity modeled with the soil geometry is varied to assess the influence of the cavity on the performance of the footing. The results of analyses are presented in 2D charts. The horizontal and vertical distances are normalized to R and H, the horizontal and vertical dimensions of the plastic mechanism beneath the footing in soil without cavities. The influence of cavity geometry, and soil types are highlighted. The failure modes observation revealed that there is a strong dependency on the soil types and cavity location. An equation of the zone of influence taking into account the parameters of the strength of the soils as well as the other the geometry related parameters.

- In Chapter 4, the investigation on the Bearing Capacity of the unsaturated soils with cavities was undertaken. The van Genuchten model was used for the SWCC model. The simulations assumed initial conditions as fully saturated and analysis simulating water drawdowns until the establishment of the steady state was conducted. The analyses illustrated several pressure head distributions which show the several levels of matric suction generated. The analysis of UBC yields similar results to dry conditions cases. However, Noticeable changes in the failure modes were observed. The influence zone expanded more due to porewater distribution and an equation of its assessment is proposed.

- In Chapter 5, based on experimental analysis, the model tests of footing on sandy soil with cavities in dry and unsaturated soils were used. Due to its availability, the silica sand No.7 was used. A new experimental approach using the balloon to simulate the cavity is introduced. The cavity's initial stages of development and its influence on the bearing capacity of the footing are investigated through the implemented model tests. The unsaturated conditions are created by initial saturation of the soil with upward injection and then, desaturation by air pressure application. The results of the analysis confirmed the trend of the numerical analysis results and thus, the experimental method.

6.2 Main findings

The study's main findings lie in an attempt to propose a new and generalized equation of the zone of influence of the cavities. Previous studies which have discussed the issue were more or less focused on specific locations. In addition, some studies were limited to marking the zone through charts without a specific way of mathematically expressing the stability level. This study, in addition, has the merit of introducing a new approach to the bearing capacity of footing on soil with cavities under unsaturated soils. To our best knowledge, no researchers have analyzed the issue of underground cavity influence under assumptions of unsaturated conditions. The most pertinent finding is the proposal of the equation of the influence zone.

This equation proposed takes into account the parameters of geometrical properties of the cavity, the footing, and the soil's strength parameters. This equation proposed is meaningful to the scientific community as well as the geotechnical engineer's practitioner that it would be in practical engineering in the investigation of subsurface sites, and prevention of collapse of engineering structures in areas prone to sinkhole or cavity development.

6.3 Future research

This thesis contributes to the knowledge of the influence of underground cavities on the bearing capacity of footing on soils with cavities in dry and unsaturated conditions. Even though, several aspects that might lead to limitations of the proposed equations are left and still need to be researched. The following are recommended for future studies:

- The analysis with RPFEM used in the present study with the Drucker-Prager is reliable. However, by assuming the associated flow rule through numerical analyses, there is a risk of overestimating the UBC and the parameters R and H because of a large dilatancy angle used in the cases of soils with large frictional angle. So, it is necessary to conduct analyses cases considering the non-associated flow rule analysis and improve the proposed equations.
- It is also important to evaluate the influence of additional parameters such as the unit weight, footing width B, seepage analysis parameters, etc. to be able to predict for wide range of soil materials and thus, reduce limitations of the proposed equations.
- In the unsaturated conditions, the simulations were conducted by adopting the van Genuchten model for the soil water characteristics curve. Even though it has proven simplicity in the application, recent developments in Unsaturated soil mechanics provide more recent SWCC models to investigate hydraulic conditions and assessment of negative porewater pressure. Thus, future improvement of the RPFEM for unsaturated flow analysis with more recent SWCC models (Fredlund et al., 2012) can be investigated in the future.
- The experimental model tests produced interesting results and confirmed the numerical analysis. However, the analysis was conducted on small-scale soil and

uniquely used one type of soil sand (Silica sand No. 7). The future works should investigate using other soil materials. In addition, the experimental device can be improved with direct tools to measure negative porewater pressure. In addition, the process of cavity creation can be improved to maintain the accuracy of the shape and size of the desired geometry, and more importantly enhance smooth reproductibility.

REFERENCES

A. Garakani, A., Sadeghi, H., Saheb, S., Lamei, A. (2020). Bearing Capacity of Shallow Foundations on Unsaturated Soils: Analytical Approach with 3D Numerical Simulations and Experimental Validations. *International Journal of Geomechanics*, *20*(3).

Ali, H., Choi, J. H. (2020). Risk prediction of sinkhole occurrence for different subsurface soil profiles due to leakage from underground sewer and water pipelines. *Sustainability (Switzerland)*, *12*(1).

Allan Freeze, R., Cherry, J. A. (1977). Groundwater. Prentice-Hall.

Al-Tabbaa A., Russell L., O'Reilly M. (1989). Model tests of footings above shallow cavities. *Ground Engineering*, *22*(7), 39–42.

Anand, A., Sarkar, R. (2022). A comprehensive probabilistic investigation on bearing behavior of unsaturated fly ash deposits. *Arabian Journal of Geosciences*, *15*(4), 369.

Atkinson, J. H., Potts, D. M. (1977). Stability of a shallow circular tunnel in cohesionless soil. *Geotechnique*, *27*(2).

Augarde, C. E., Lyamin, A. V, Sloan, S. W., (2003). Prediction of Undrained Sinkhole Collapse. *Journal of Geotechnical and Geoenvironmental Engineering*, *129*(3), 197–205.

Badie, A., Wang, M. C. (1984). Stability of spread footing above void in clay. *J. Geotech. Eng.*, *110*(11), 1591–1605.

Baus, R. L., Wang, M. C. (1983). Bearing capacity of strip footing above void. *Journal of Geotechnical Engineering*, *109*(1), 1–14.

Cascone, E., Biondi, G., Casablanca, O. (2021). Groundwater effect on bearing capacity of shallow strip footings. *Computers and Geotechnics*, *139*.

Chandler, N. A., DeJong, J. T. (2008). Subsurface explorations for slope stability analysis. *Journal of Geotechnical and Geoenvironmental Engineering*, *134*(2), 139–150.

Corkum, B., Hoek, E., Carranza-Torres, C., Hoek, E., Carranza-Torres, C., Corkum, B. (2002). *Hoek-Brown failure criterion-2002 Edition* (Vol. 1).

Costa, Y. D., Cintra, J. C., Zornberg, J. G. (2003). Influence of matric suction on the results of plate load tests performed on a lateritic soil deposit. *Geotechnical Testing Journal*, *26*(2).

Culver, D. C., Pipan, T., Schneider, K. (2019). *The Biology of Caves and Other Subterranean Habitats* (Oxford University Press, Ed.; 2nd ed.).

Davis, E. H., Gunn, M. J., Mair, R. J., Seneviratne, H. N. (1980). The stability of shallow tunnels and underground openings in cohesive material. *Geotechnique*, *30*(4).

Drumm, E. C., Aktürk, Ö., Akgün, H., Tutluoğlu, L. (2009). Stability Charts for the Collapse of Residual Soil in Karst. *Journal of Geotechnical and Geoenvironmental Engineering*, *135*(7).

Duncan, J. M. (1996.). State of the art: limit equilibrium and finite-element analysis of slopes. *Journal of Geotechnical Engineering,* 122(7),557-596.

Ford, D., Williams, P. (2007). *Karst Hydrogeology and Geomorphology* (John Wiley & Sons,).

Foster, M., Fell, R., Spannagle, M. (2000). *The statistics of embankment dam failures and accidents*.

Fredlund, D. G., Rahardjo, H. (1993). Soil Mechanics for Unsaturated Soils. In *Soil Mechanics for Unsaturated Soils*. John Wiley & Sons.

Fredlund, D. G., Rahardjo, H., Fredlund, M. D. (2012). Unsaturated soil mechanics in engineering practice. John Wiley and Sons, Hoboken, NJ. 926p. In *Unsaturated Soil Mechanics in Engineering Practice*.

Ghasemzadeh, H., Akbari, F. (2019). Determining the bearing capacity factor due to nonlinear matric suction distribution in the soil. *Canadian Journal of Soil Science*, *99*(4), 434–446.

Goodman, R. E. (1989). *Introduction to rock mechanics* (John Wiley & Sons Ed.; Second Edition).

Guo, S., Shao, Y., Zhang, T., Zhu, David. Z., & Zhang, Y. (2013). Physical Modeling on Sand Erosion around Defective Sewer Pipes under the Influence of Groundwater. *Journal of Hydraulic Engineering*, *139*(12), 1247–1257.

Hermosilla, R. G. (2012). The Guatemala City sinkhole collapses. *Carbonates and Evaporites*, *27*(2), 103–107. https://doi.org/10.1007/s13146-011-0074-1.

Holzer, T. L. (2009). *Living with Unstable Ground*. American Geological Institute.

Hoshina, T., Ohtsuka, S., Isobe, K. (2011). Rigid plastic stability analysis for slope including thin weak layer. *Jiban Kogaku Journal (Japanese Geotechnical Journal)*, *6*(2).

Iqbal, T., Ohtsuka, S., Isobe, K., Fukumoto, Y., & Kaneda, K. (2023). Influence of strip footing size on the ultimate bearing capacity formula for sandy soils. *International Journal of geomate*, *24*(102).

Karl Terzaghi, Ralph B. Peck, Gholamreza M. (1996). Soils mechanics in Engineering practice.

Keawsawasvong, S., Ukritchon, B. (2019). Undrained stability of a spherical cavity in cohesive soils using finite element limit analysis. *Journal of Rock Mechanics and Geotechnical Engineering*, *11*(6), 1274–1285.

Khadka, S. (2018). *A numerical study of the coupled geomechanical processes in sinkholes*. University of Toledo.

Kiyosumi, M., Kusakabe, ; Osamu, Ohuchi, ; Masatoshi, & Le Peng, F. (2007). *Yielding Pressure of Spread Footing above Multiple Voids*.

Kiyosumi, M., Kusakabe, O., Asce, M., & Ohuchi, M. (2011). Model Tests and Analyses of Bearing Capacity of Strip Footing on Stiff Ground with Voids.

Kuwano, R. (2021). *Subsurface cavities and road cave-ins*. IPA news letter(6).

Leca, E., Dormieux, L. (1990). Upper and lower bound solutions for the face stability of shallow circular tunnels in frictional material. *Geotechnique*, *40*(4).

Lee, J. K., Jeong, S., Ko, J. (2014). Undrained stability of surface strip footings above voids. *Computers and Geotechnics*, *62*.

Lee, J. K., Kim, J. (2019). Stability charts for sustainable infrastructure: Collapse loads of footings on sandy soil with voids. *Sustainability (Switzerland)*, *11*(14).

Machel, H. G., Mountjoy, E. W. (1986). Dolomite—a useful model for the origin of evaporite brines. *Journal of Sedimentary Research*, *5*(3), 289–303.

Mühlhaus, H. B. (1985). Lower bound solutions for circular tunnels in two and three dimensions. *Rock Mechanics and Rock Engineering*, *18*(1).

Mukunoki, T., Kumano, N., & Otani, J. (2012). Image analysis of soil failure on defective underground pipe due to cyclic water supply and drainage using X-ray CT. *Frontiers of Structural and Civil Engineering*, *6*(2).

Nguyen, D. L., Ohtsuka, S., Hoshina, T., Isobe, K. (2016). Discussion on size effect of footing in ultimate bearing capacity of sandy soil using rigid plastic finite element method. *Soils and Foundations*, *56*(1).

Nygren, M., Giese, M., Kløve, B., Haaf, E., Rossi, P. M., Barthel, R. (2020). Changes in seasonality of groundwater level fluctuations in a temperate-cold climate transition zone. *Journal of Hydrology X*, *8*, 100062.

Oh, W. T., Vanapalli, S. K. (2013). Interpretation of the Bearing Capacity of Unsaturated Fine-Grained Soil Using the Modified Effective and the Modified Total Stress Approaches. *International Journal of Geomechanics*, *13*(6), 769–778.

Palmer, N. P. (2007). *Cave Geology*. KIP Articles. 775.

Parise, M., Gunn, J. (2007). Natural and Anthropogenic Hazards in Karst Areas: Recognition, Analysis and Mitigation. In *Environmental & Engineering Geoscience* - (Vol. 16).

Pham, Q. N., Ohtsuka, S., Isobe, K., Pham, V. N., Hoang, H. P. (2023). Limit load space of rigid strip footing on sand slope subjected to combined eccentric and inclined loading. *Computers and Geotechnics*, *162*.

Renfrew, C., Bahn, P. (2018). *Archaeology: Theories, Methods, and Practice* (Thames & Hudson., Ed.).

Rojas, J. C., Salinas, L. M., Sejas, C. (2007). Plate-Load Tests on an Unsaturated Lean Clay. In *Experimental Unsaturated Soil Mechanics*.

Sato, M., Kuwano, R. (2015). Influence of buried structures on underground seepage and generation of cavities. *Japanese Geotechnical Journal*, *10*(1), 113–125.

Shin, J. H., Addenbrooke, T. I., & Potts, D. M. (2002). A numerical study of the effect of groundwater movement on long-term tunnel behaviour. *Geotechnique*, *52*(6).

Tamura, T. (1990). Rigid Plastic Finite Element Method in Geotechnical Engineering. *Computational Plasticity, Current Japanese Material Research*, 15–23.

Tamura, T., Kobayashi, S., Sumi, T. (1984). Limit Analysis of Soil Structure by Rigid Plastic Finite Element Method. *Soils and Foundations*, *24*(1), 34–42.

Tamura, T., Kobayashi, S., Sumi, T. (1987). Rigid-plastic finite element method for frictional materials. *Soils and Foundations*, *27*(3), 1–12.

Tan, M., Cheng, X., Vanapalli, S. (2021). Simple Approaches for the Design of Shallow and Deep Foundations for Unsaturated Soils I: Theoretical and Experimental Studies. *Indian Geotechnical Journal*, *51*(1).

Tang, Y., Chen, C., Qian, B., Ren, J., Guan, Y. (2022). Plate Load Tests on an Unsaturated Sand–Kaolin Mixture with Varying Water Table. *Sensors*, *22*(6).

Tang, Y., Taiebat, H. A., Russell, A. R. (2017). Bearing Capacity of Shallow Foundations in Unsaturated Soil Considering Hydraulic Hysteresis and Three Drainage Conditions. *International Journal of Geomechanics*, *17*(6

Tang, Y., Vo, T., Taiebat, H. A., Russell, A. R. (2018). Influences of Suction on Plate Load Tests on Unsaturated Silty Sands. *Journal of Geotechnical and Geoenvironmental Engineering*, *144*(8).

Tharp, T. M. (1999). Mechanics of upward propagation of cover-collapse sinkholes. *Engineering Geology*, *52*(1–2).

Vahedifard, F., Robinson, J. D. (2016). Unified Method for Estimating the Ultimate Bearing Capacity of Shallow Foundations in Variably Saturated Soils under Steady Flow. *Journal of Geotechnical and Geoenvironmental Engineering*, *142*(4).

Vanapalli, S. K., Mohamed, F. M. O. (2013). Bearing capacity and settlement of footings in unsaturated sands. *International Journal of geomate*, *5*(1).

Varnes, D. J. (1984). Landslide hazard zonation: a review of principles and practice. United Nations.

Vo, T., Russell, A. R. (2016). Bearing capacity of strip footings on unsaturated soils by the slip line theory. *Computers and Geotechnics*, *74*.

Waltham, T., Lu, Z. (2007). Natural and anthropogenic rock collapse over open caves. *Geological Society Special Publication*, *279*.

Wang, M. C., & Hsieh, C. W. (1987). Collapse load of strip footing above circular void. *Journal of Geotechnical Engineering*, *113*(5).

Wei, L., Hudson, J. A. (1990). Permeability variation around underground opening in jointed rock masses : A numerical study. *International Symposium on Rock Joints*, 565–569.

Williams, P. W. (2004). Encyclopedia of caves and karst science. In Fitzroy Dearbon (Ed.), *Choice Reviews Online* (Gunn, John ed., Vol. 41, Issue 10). Fitzroy Dearborn.

Wu, G., Zhao, H., Zhao, M. (2021). Undrained stability analysis of strip footings lying on circular voids with spatially random soil. *Computers and Geotechnics*, *133*.

Wu, G., Zhao, M., Zhang, R., Liang, G. (2020). Ultimate bearing capacity of eccentrically loaded strip footings above voids in rock masses. *Computers and Geotechnics*, *128*.

Xiao, Y., Zhang, M., Zhou, Z., Hou, Z., Lv, J., Tang, M., & Zhang, R. (2023). Ultimate bearing capacity of strip footings above rectangular voids in Hoek-Brown rock masses. *Computers and Geotechnics*, *161*.

Yamamoto, K., Lyamin, A. V., Wilson, D. W., Sloan, S. W., Abbo, A. J. (2013). Stability of dual circular tunnels in cohesive-frictional soil subjected to surcharge loading. *Computers and Geotechnics*, *50*.

Yan, E., Cheng, J., Liu, L. (2009). Stability Analysis and Evaluation of Soil Cave Foundation under the role of Groundwater in Karst Area. *International Journal of Intelligent Systems and Applications*, *1*(1).

Zhao, L., Huang, S., Zeng, Z., Zhang, R., Tang, G., Zuo, S. (2021). Study on the ultimate bearing capacity of a strip footing influenced by an irregular underlying cavity in karst areas. *Soils and Foundations*, *61*(2), 259–270.

Zhou, H., Zheng, G., He, X., Xu, X., Zhang, T., Yang, X. (2018). Bearing capacity of strip footings on c–φ soils with square voids. *Acta Geotechnica*, *13*(3), 747–755.

Zhou, W., Beck, B. F. (2008). Management and mitigation of sinkholes on karst lands: An overview of practical applications. *Environmental Geology*, *55*(4).